Mesoscale Band Formation in Three Major Northeastern United States Snowstorms

DAVID J. NICOSIA AND RICHARD H. GRUMM

NOAA/National Weather Service, State College, Pennsylvania

(Manuscript received 15 May 1998, in final form 2 November 1998)

ABSTRACT

The National Centers for Environmental Prediction's 29-km version Meso Eta Model and Weather Surveillance Radar-1988 Doppler base reflectivity data were used to diagnose intense mesoscale snowbands in three northeastern United States snowstorms. Snowfall rates within these snowbands were extreme and, in one case, were close to 15 cm (6 in.) per hour. The heaviest total snowfall with each snowstorm was largely associated with the positioning of these mesoscale snowbands. Each snowstorm exhibited strong midlevel frontogenesis in conjunction with a deep layer of negative equivalent potential vorticity (EPV). The frontogenesis and negative EPV were found in the deformation zone, north of the developing midlevel cyclone. *Cross-sectional analyses (oriented perpendicular to the isotherms) indicated that the mesoscale snowbands formed in close correlation to the intense midlevel frontogenesis and deep layer of negative EPV.*

It was found that the EPV was significantly reduced on the warm side of the midlevel frontogenetic region as midlevel dry air, associated with a midlevel dry tongue jet, overlaid a low-level moisture-laden easterly jet, north of each low-level cyclone. The continual reduction of EPV on the warm side of the frontogenetic region is postulated to have created the deep layer of negative EPV in the warm advection zone of each cyclone. The negative EPV was mainly associated with conditional symmetric instability (CSI). Each case exhibited a much smaller region of conditional instability (CI) on the warm side of the frontogenesis maximum for a short period of time. The CSI and, to a lesser extent, CI are postulated to have been released as air parcels ascended the moist isentropes, north of the warm front, upon reaching saturation. This likely was a major factor in the mesoscale band formation and heavy snowfall with each snowstorm.

The results indicate that model frontogenesis and EPV fields can be used to predict the potential development of mesoscale snowbands. When a deep layer of negative EPV and strong midlevel frontogenesis are forecast by the models, forecasters can anticipate the regions where mesoscale snowbands may form. Inspection of saturation equivalent potential temperature in conjunction with EPV is suggested to determine whether CI is present in a negative EPV region. If CI is present in addition to CSI, then upright convection may dominate over slantwise convection leading to heavier snowfall rates. The region where the frontogenesis and negative EPV are forecast to persist the longest (usually left of the 700-hPa low track) is where the heaviest storm total snowfall will occur. Once mesoscale bands are detected on radar, accurate short-term forecasts of areas that will receive heavy snowfall can be made.

1. Introduction

The roles of conditional symmetric instability (CSI) and frontogenesis in producing mesoscale precipitation bands have been extensively studied (e.g., Bennetts and Hoskins 1979; Emanuel 1979, 1983; Sanders and Bosart 1985; Sanders 1986; Wolfsberg et al. 1986; Moore and Blakeley 1988; Shields et al. 1991). There is evidence that frontogenesis and CSI may work in concert to produce mesoscale precipitation bands in extratropical cyclones. Sanders and Bosart (1985), Sanders (1986), and Wolfsberg et al. (1986) all showed that both frontogenesis and CSI (and/or low moist symmetric stability) were present during major northeastern United States snowstorms that possessed mesoscale snowbands. Additionally, Emanuel (1985) proposed a coupled dynamical relationship between frontogenesis and moist symmetric stability for producing mesoscale precipitation bands. He showed that ascent associated with frontogenesis was enhanced and constricted to a smaller scale when the symmetric stability was low on the warm side of the developing frontal zone. Furthermore, Xu (1989) showed, theoretically, that frontogenesis in the presence of CSI can lead to long-lived mesoscale precipitation bands.

The tendency for heavy snowfall in major snowstorms to occur from mesoscale precipitation bands presents a challenge to forecasters. In the past, the resolution of the operational numerical weather prediction models was too coarse to resolve mesoscale circulations associated with banded precipitation. Sanders (1973) and Bosart (1975) suggested that improvements in pre-

Corresponding author address: David J. Nicosia, National Weather Service Office, 227 W. Beaver Ave., Suite 402, State College, PA 16801.
E-mail: nicosia@supercel.met.psu.edu

dicting precipitation from synoptic-scale models was hampered due to the importance of mesoscale processes on the distribution and intensity of precipitation. In the case examined by Moore and Blakeley (1988), the snowfall was not well forecast by operational meteorologists and termed a ''surprise'' event. This undoubtedly was due to the narrowness of the heavy snowfall distribution and the coarser resolution of the operational models in the 1980s.

With finer-resolution mesoscale models becoming more available to the operational forecast environment (e.g., 29-km Meso Eta Model), diagnosing vertical motion associated with mesoscale processes is improving. The Meso Eta showed higher skill in forecasting precipitation when compared to its synoptic counterpart, the 80-km Eta (Black 1994). Black showed that the Meso Eta simulated a mesoscale precipitation band behind a cold front that the coarser-resolution synoptic Eta Model failed to capture. Since frontogenesis typically produces bands of precipitation on the order of 50 km wide (Browning 1985), the resolution of the 29-km Meso Eta should improve simulation of frontogenetic forcing within synoptic-scale snowstorms but still may not adequately resolve the character of the mesoscale precipitation bands.

With the modernization of the National Weather Service (NWS), new technologies have become available to better observe and forecast mesoscale banded precipitation events. The deployment of the Weather Surveillance Radar-1988 Doppler (WSR-88D) nationwide has allowed forecasters to better detect banded precipitation events (Dankers 1994; Grumm and Nicosia 1997). In addition, gridded model output in NWS offices has vastly improved forecaster's abilities to diagnose vertical motion and obtain a better understanding of atmospheric processes (Dunn 1991; Wiesmueller and Brady 1993; Nicosia 1995). With gridded model output available at NWS offices, frontogenesis and CSI can be diagnosed operationally and incorporated into the forecast process (Wiesmueller and Zubrick 1998).

The purpose of this paper is to examine mesoscale snowband formation for three northeastern United States snowstorms using the Meso Eta Model and WSR-88D data. The Meso Eta will be used to diagnose the frontogenesis, moist symmetric stability, CSI, and conditional instability (CI) with each snowstorm in the vicinity of the mesoscale snowbands detected by the WSR-88D. The use of frontogenesis, moist symmetric stability, CSI, and conditional instability (CI) for the prediction of heavy snow will be stressed.

Specifically, the paper is divided into five sections. The next section (section 2) discusses the data and methodology employed and provides an overview of frontogenesis, and the use of equivalent potential vorticity (EPV) for diagnosing moist symmetric stability, CSI, and CI. The generation and reduction of EPV in extratropical cyclones is also discussed in section 2. Section 3 presents the three snowstorm case studies. The discussion section (section 4) presents a conceptual model for mesoscale snowband formation and discusses the use of model frontogenesis and EPV for forecasting heavy snow. The last section (section 5) summarizes the results of this study, and provides concluding remarks and suggestions for future work.

2. Data and methodology

a. Data

WSR-88D radar data (Klazura and Imy 1993) and Meso Eta Model frontogenesis and EPV fields were examined for three major snowstorms in Pennsylvania and New York State. The snowstorms occurred on the following dates: 4–5 February 1995, 14–15 November 1995, and 12–13 January 1996. The snowstorms were chosen based on the availability of radar, model, and observational data. Cases were also selected based on the similarities between snowstorms. Each snowstorm displayed an extensive low-level cyclone in the vicinity of the northeast United States and middle Atlantic coasts. Furthermore, for two of the three snowstorms, cyclogenesis was occurring as the distance between the upper-level trough axis and low-level cyclone was decreasing. These two cases exhibited surface cyclones that deepened at least 15 hPa in 24 h. All three snowstorms had heavy snowfall in the northwest or ''comma head'' portion of the cyclone.

To examine the intensity of the snowfall over Pennsylvania and New York, base reflectivity data from the 0.5° elevation slice was obtained from the following WSR-88D sites: central Pennsylvania (KCCX); Binghamton, New York (KBGM); Albany, New York (KENX); Pittsburgh, Pennsylvania (KPBZ); Sterling, Virginia (KLWX); Fort Dix, New Jersey (KDIX); and Brookhaven, New York (KOKX). WSR-88D data was limited for the 12–13 January 1996 snowstorm, being available only from KBGM.

Snowfall data was obtained from cooperative observers and snow spotters from the NWS, and official NWS observations. Station plots and buoy data were obtained from the NWS in State College, Pennsylvania, and from The Pennsylvania State University meteorological system (Cahir et al. 1981). Buoy data was available for two of the three cases. All time references in this paper will use date and universal coordinated time (UTC) in the following form: 14/0000 UTC, which stands for the 14th at 0000 UTC.

The Meso Eta Model grids were examined for each snowstorm using General Meteorological Package (GEMPAK) 5.4 (desJardines et al. 1991). The model forecasts were available every 3 h for two of the cases (14–15 November 1995 and 12–13 January 1996) and every 6 h for the other case (4–5 February 1995). The model data was interpolated to a 40-km grid. Unfortunately, model precipitation forecasts were not avail-

able for any case. The Meso Eta Model fields were used for the synoptic analysis of each case study in section 3.

b. Frontogenesis and equivalent potential vorticity calculations

The process of frontogenesis can be defined mathematically as

$$F = \frac{1}{|\nabla_p \theta|}\left[-\left(\frac{\partial\theta}{\partial x}\right)^2\frac{\partial u}{\partial x} - \frac{\partial\theta}{\partial y}\frac{\partial\theta}{\partial x}\frac{\partial v}{\partial x} - \frac{\partial\theta}{\partial x}\frac{\partial\theta}{\partial y}\frac{\partial u}{\partial y} - \left(\frac{\partial\theta}{\partial y}\right)^2\frac{\partial v}{\partial y}\right] \quad (1)$$

and is known as the two-dimensional (2D) scalar frontogenetic function from Petterssen (1956). This frontogenetic function is defined as the Lagrangian rate change of the magnitude of the *horizontal* potential temperature gradient due to the horizontal wind. When the potential temperature gradient increases, frontogenesis is implied; when the gradient decreases, frontolysis is implied.

The frontogenetic function defined in (1) is based on shearing and stretching deformation of the horizontal wind field and its action on the horizontal potential temperature gradient. When the angle between the axis of dilatation and the isotherms is between 0° and 45°, the deformation of the wind field acts to increase the horizontal potential temperature gradient, implying frontogenesis. The maximum frontogenesis occurs when the dilatation axis and the isotherms are parallel.

A local increase in the potential temperature gradient through deformation of the wind has dynamic consequences. An increase in the potential temperature gradient leads to a disruption of thermal wind balance since the horizontal temperature gradient becomes too large for the associated vertical wind shear. To restore thermal wind balance, the atmosphere produces a thermally direct ageostrophic circulation transverse to the baroclinic zone (Koch 1984; Sanders and Bosart 1985). Thus, frontogenesis leads to vertical motion by inducing a *thermally direct ageostrophic circulation.*

Frontogenesis was computed from the built-in GEMPAK frontogenetic function, which is defined mathematically in (1). In this paper, scalar 2D frontogenesis will simply be referred to as frontogenesis. Frontogenesis was calculated from GEMPAK 5.4 using total winds (geostrophic plus ageostrophic) instead of the geostrophic winds alone because the ageostrophic winds are important near frontal zones, especially strong frontal zones (Hoskins and Bretherton 1972; Barnes 1985; Jascourt et al. 1988; Ruscher and Condo 1996). The frontogenetic function was compared to the WSR-88D radar reflectivity imagery for the three snowstorms to investigate the role of frontogenesis in mesoscale snowband formation.

To assess the moist symmetric stability with each case, EPV was calculated from a built-in GEMPAK function in cross sections normal to the isotherms. EPV is defined as

$$\text{EPV} = g\left[\underbrace{\left(\frac{\partial M_g}{\partial p}\frac{\partial\theta_{es}}{\partial x}\right)}_{\text{A}} - \underbrace{\left(\frac{\partial M_g}{\partial x}\frac{\partial\theta_{es}}{\partial p}\right)}_{\text{B}}\right], \quad (2)$$

with the x direction representing the direction perpendicular to the thermal wind with x increasing in the direction of the warmer air (Moore and Lambert 1993). Note that the EPV was calculated using geostrophic momentum (M_g), which is defined as $M_g = V_g + fx$, and saturation equivalent potential temperature (θ_{es}).

It can be shown from (2) that, in a baroclinic atmosphere, *CSI is present when EPV is negative.* Term A represents the contribution to EPV from the vertical wind shear and the horizontal temperature gradient. When the temperature increases in the x direction ($\partial\theta_{es}/\partial x > 0$), the wind will increase with height (or increase with decreasing pressure) and $\partial M_g/\partial p$ will be less than zero. Thus, when the vertical wind shear and associated horizontal temperature gradient are large, $\partial M_g/\partial p$ will be more negative with the M_g surfaces attaining a more shallow slope in the x–p plane. The contribution to EPV from term A in this case will be more negative and there is a better chance that θ_{es} will slope more steeply than the M_g surfaces, a necessary condition for CSI. It is easy to see that this is favored when low static stability (θ_{es} is steeply sloped in the x–p plane) is present ($\partial\theta_{es}/\partial p$ is a small, negative number). Since $\partial M_g/\partial x$ (the absolute vorticity) is almost always positive, term B will be a smaller negative number than term A and EPV will tend to be negative.

It is also possible that CI can be present in conjunction with CSI when the EPV is negative. If a layer is moist statically unstable (θ_{es} decreasing with height or $\partial\theta_{es}/\partial p > 0$), then term B will be positive and contribute to negative EPV when CSI is present. In a baroclinic environment, term A is always negative, and it is easy to see how CSI and CI can coexist.

When a layer contains negative EPV, it is important to understand that for CSI and/or CI to be released, the layer must be saturated with ascent present. When CSI and CI are present, it is expected that upright convection will dominate from the release of CI over the slantwise convection associated with the release of CSI. It is also possible that the release of CSI may trigger the release of CI, resulting in upright convection (Bennetts and Sharp 1982; Xu 1986). Thus, for slantwise convection to occur, *the atmosphere must be statically stable ($\partial\theta_{es}/\partial p < 0$) within a region of negative EPV.* This assumes saturated conditions exist in the presence of vertical motion. To assess the potential for CSI and CI within negative regions of EPV, θ_{es} surfaces were examined for each case in conjunction with the EPV.

To examine the time evolution of the frontogenesis, moist symmetric stability and static stability with each snowstorm, cross sections of the frontogenetic function

(1), EPV (2), vertical velocity, the ageostrophic vertical circulation, θ_{es}, and M_g were examined for various stages of cyclogenesis for each storm. The cross sections were taken north of each surface low perpendicular to the 700-hPa isotherms at various forecast times moving northeast with each surface low. The 700-hPa level was chosen for the frontogenesis calculations (in the x–y plane) since a distinct maximum in frontogenesis formed near 700 hPa in the cross sections with each case.

To assess the EPV tendency with each case, a generation term for EPV was examined. It can be shown, for frictionless and adiabatic flow, that the generation of EPV can be given by the following equation [adapted from Bennetts and Hoskins (1979) and Bluestein (1993)]:

$$\frac{d(\text{EPV})}{dt} = \frac{g[k \cdot (\nabla\theta_e \times \nabla\theta)]}{\rho\overline{\theta}}, \qquad (3)$$

where $\overline{\theta}$ is an average value of θ in the midtroposphere. Equation (3) states that the EPV will be reduced when the gradient of θ_e lies within 90° of, and to the left of, the gradient of θ. Physically, this means that EPV will be reduced in a region where the moisture gradient lies in the same direction as the thermal wind vector (see Bluestein 1993 for details). This ''setup'' is commonly found in the vicinity of a low-level cyclone embedded in a baroclinic zone with the colder air to the north. Moisture-laden air [i.e., warm conveyor belt; Carlson (1980)] is typically found on the east side of a developing extratropical cyclone with drier air to the west. Since the colder air lies to the north, the thermal wind is westerly and points in the same direction as the moisture gradient (to the east). Since there is an increase in westerly flow in the vertical, drier air is preferentially advected above moist air in the low levels. The effect of this is to steepen the θ_e surfaces, which lowers the EPV by term B in (2). Where the temperature gradient is largest, the differential moisture advection will be most pronounced due to stronger vertical wind shear. Thus, a reduction in EPV will be favored in frontogenetic regions, which are characterized by increasing temperature gradients and vertical wind shear.

It is easy to see from (3) that frontogenesis, by leading to an increase in the temperature gradient, leads to a reduction in the EPV. This assumes the moisture gradient lies in the same direction as the thermal wind and saturation does not exist. With smaller EPV on the warm side of a frontogenetic region, the vertical motion associated with frontogenesis is enhanced and reduced to a smaller scale (Emanuel 1985). An underlying assumption associated with the frontogenetic function is that the flow is two-dimensional with the horizontal axis perpendicular to the isotherms. Thus, enhanced vertical motion from frontogenesis occurs parallel to the isotherms with the enhanced low-level ageostrophic winds oriented perpendicular to the isotherms. This leads to stronger ageostrophic advection of temperature, which, in turn, increases the temperature gradient and associated frontogenesis. An increase in the temperature gradient further reduces the EPV by (3) and a nonlinear process continues, which increases the frontogenesis and reduces the EPV. In this way, it is postulated that negative EPV can develop in close association to a frontogenetic region during cyclogenesis.

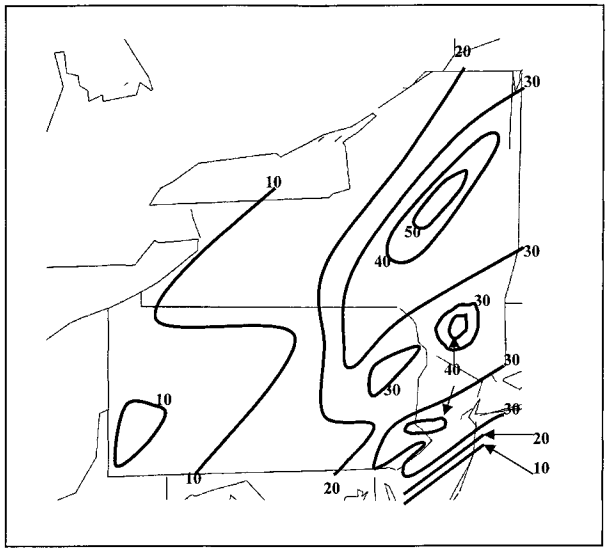

FIG. 1. Total snowfall (cm) for 4 and 5 Feb 1995 over Pennsylvania, New York, and New Jersey. Snowfall amounts under 10 cm were excluded. Contour interval every 10 cm.

3. Case studies

a. The 4–5 February 1995 northeastern United States snowstorm

On 4–5 February 1995, a snowstorm affected portions of Pennsylvania, New York, New Jersey, and New England. Figure 1 shows the total snowfall for 4–5 February 1995 over Pennsylvania, New York, and New Jersey. Figure 2 shows the 300- and 1000-hPa geopotential heights as depicted by the 4/0000 UTC Meso Eta forecast cycle. At 4/0600 UTC, there were two 1000-hPa low centers, one over West Virginia and another developing in the vicinity of the Carolinas (Fig. 2a). Between 4/0600 UTC and 4/1200 UTC, a sharp 300-hPa trough axis moved from the western Great Lakes and lower Mississippi Valley to a position from Lower Michigan south through the Ohio and Tennessee Valleys (Figs. 2a and 2b). Between 4/1200 UTC and 5/0000 UTC, the Carolina 1000-hPa low deepened significantly, becoming the primary low-level cyclone as it tracked to southern New England (Figs. 2b–d). The Ohio Valley 1000-hPa low filled by 4/1200 UTC. The 300-hPa trough axis became negatively tilted and advanced relative to the low-level cyclone indicative of cyclogenesis between 4/1200 UTC and 5/0000 UTC (Figs. 2b–d).

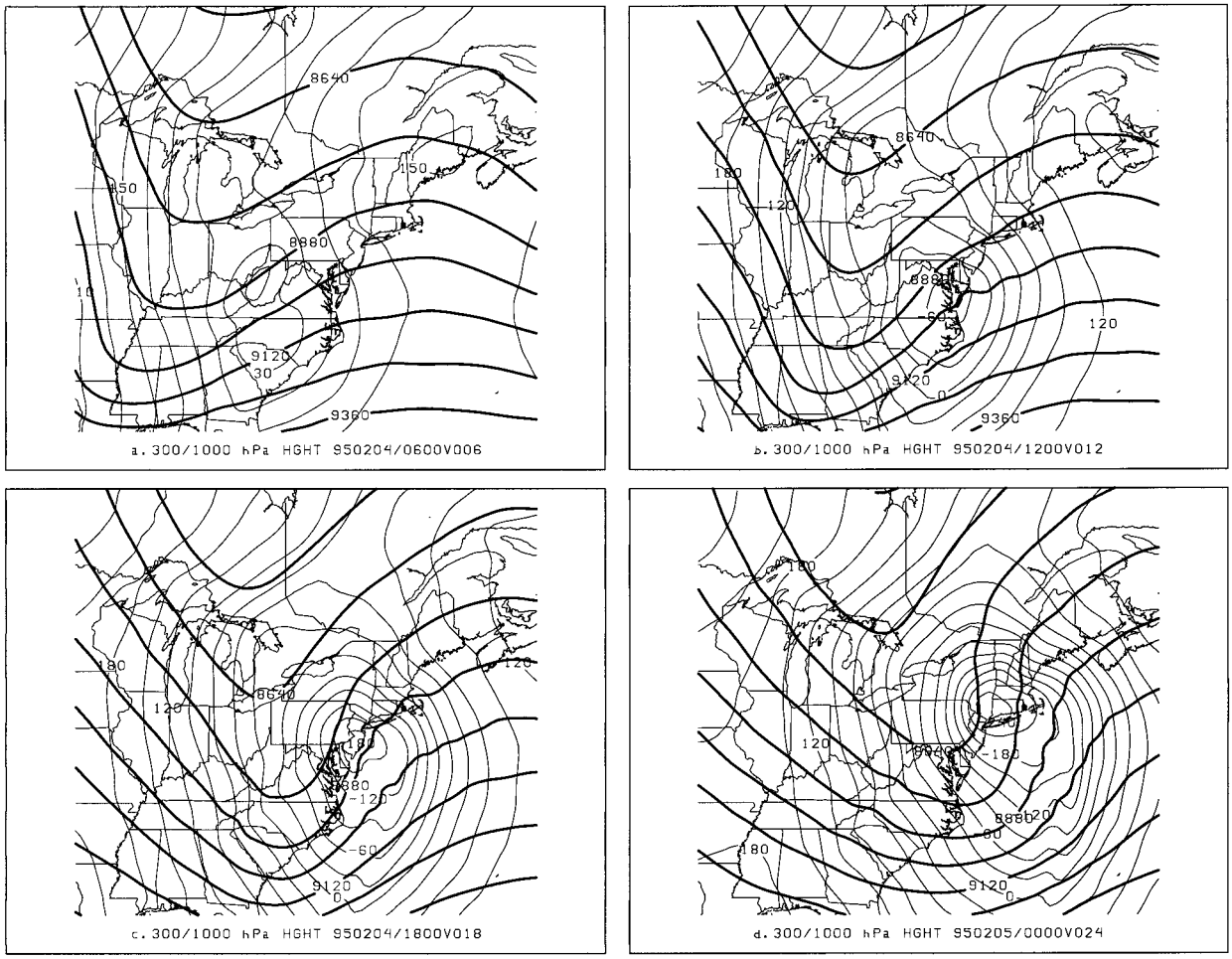

FIG. 2. The Meso Eta forecast 300-hPa geopotential heights (dark, 120-m interval), and 1000-hPa geopotential heights (light, 30-m interval) for (a) 6-h forecast valid 0600 UTC 4 Feb 1995, (b) 12-h forecast valid 1200 UTC 4 Feb 1995, (c) 18-h forecast valid 1800 UTC 4 Feb 1995, and (d) 24-h forecast valid 0000 UTC 5 Feb 1995.

Figure 3 shows the KENX WSR-88D base reflectivity during the height of the snowstorm at 4/1801 UTC. A well-defined mesoscale snowband was oriented northeast to southwest from west-central Vermont to south-central New York State, northeast of Binghamton, New York. Snowfall rates within this snowband were reported to be 10 cm (4 in.) h^{-1} at times from NWS spotter reports. This mesoscale snowband previously was oriented in a west-to-east direction from northeastern Pennsylvania to Long Island, New York, at 4/1200 UTC (not shown) in association with strong warm air advection ahead of the 1000-hPa low. The mesoscale snowband intensified while rotating counterclockwise as it moved into upstate New York. The band was positioned to the left of the eventual Meso Eta 700-hPa low track (Fig. 4), which allowed it to pivot over locations in eastern New York. As a result, the heaviest storm total snowfall was found in eastern New York State and largely associated with this mesoscale snowband (cf. Figs. 1 and 3).

Figure 4 shows the Meso Eta 4/1200 UTC forecast cycle 0–24-h forecast of the 700-hPa geopotential height and frontogenetic function. Initially, a 700-hPa trough existed across the middle Atlantic states with a band of frontogenesis oriented west-to-east, north of the 1000-hPa low (Fig. 4a). In time, as the 700-hPa low emerged from the trough, the band of frontogenesis intensified and remained north of the 700-hPa low (Figs. 4b and 4c). The frontogenesis was strongest at this stage. Likewise, the mesoscale snowband reached its greatest intensity at these time periods and was closely correlated to the 700-hPa frontogenesis band at this time (cf. Figs. 3 and 4b). Eventually, the band of frontogenesis weakened and moved to the west of the 700-hPa low (Fig. 4d). It was at this time that the low-level cyclone was almost directly underneath the middle- and upper-level lows (not shown).

Cross sections of both frontogenesis, EPV, and θ_{es} are shown in Fig. 5 for the corresponding model forecasts and cross-section endpoints as depicted in Fig. 4. Ini-

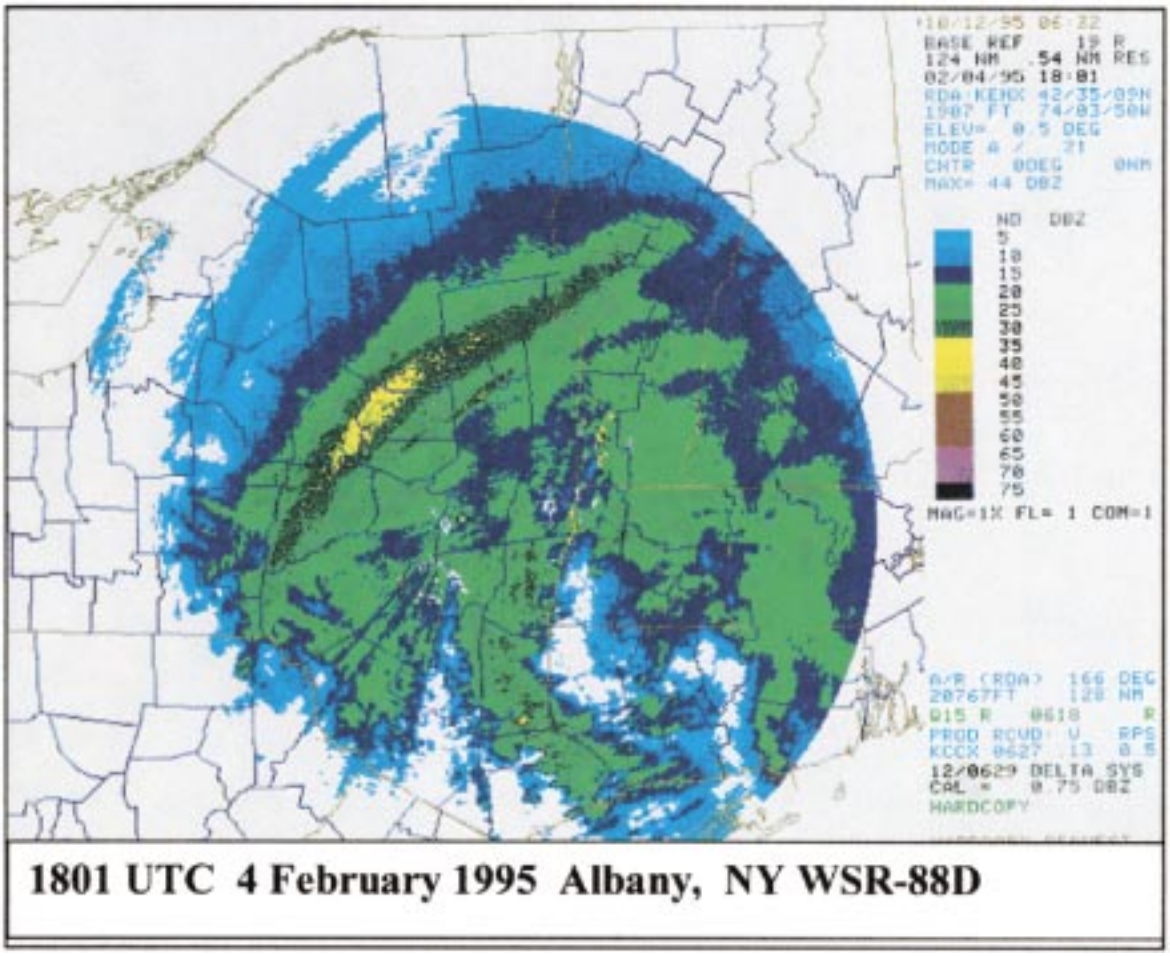

FIG. 3. KENX WSR-88D base reflectivity (0.5° elevation) at 1801 UTC 4 February 1995 (color scale to the right of the image, every 5 dBZ).

tially, a sloped layer of frontogenesis was present in conjunction with an area of negative EPV (Fig. 5a). The negative EPV was mainly associated with CSI. There was a small layer of CI present roughly between 650 and 550 hPa above the frontogenesis region (Fig. 5a). As the 700-hPa low and frontogenesis band (in the x–y plane) developed, an isolated maxima in frontogenesis emerged near 700 hPa in conjunction with a deep layer of negative EPV (Figs. 5b and 5c). In addition, the EPV grew more negative at these times, which was at the height of mesoscale snowband formation. The θ_{es} fields indicates that this region of highly negative EPV was entirely CSI (Figs. 5b and 5c). Figure 5d indicates that the EPV at 5/1200 UTC became positive through most of the troposphere in conjunction with a much weaker region of frontogenesis to the west of the cyclone center. It was at this time that the associated model vertical motions weakened as the low-level cyclone became nearly collocated with the middle- and upper-level lows.

It is apparent that a synergistic relationship between frontogenesis and EPV was present in the Meso Eta Model fields. As the frontogenesis increased north of the low-level cyclone, the EPV grew more negative. A large mesoscale snowband developed and was associated with intense midlevel frontogenesis and a region of highly negative EPV. This case illustrates that the development of a midlevel frontogenesis maximum in conjunction with a highly negative region of EPV from model forecasts *indicates the potential for heavy snowfall and mesoscale snowbands.*

b. The 14–15 November 1995 Pennsylvania snowstorm

On 14 and 15 November 1995, a major early season winter storm dumped up to 70 cm (27.6 in.) of snow in the mountains of western Pennsylvania (Fig. 6). The rain–snow line with this storm was positioned roughly across the central part of Pennsylvania and extended from Elmira, New York, south to Chambersburg, Pennsylvania. Where the heaviest storm total snow fell, the precipitation was entirely in the form of snow.

Figure 7 shows the 300- and 1000-hPa geopotential heights from the 14/1500 UTC Meso Eta Model forecast

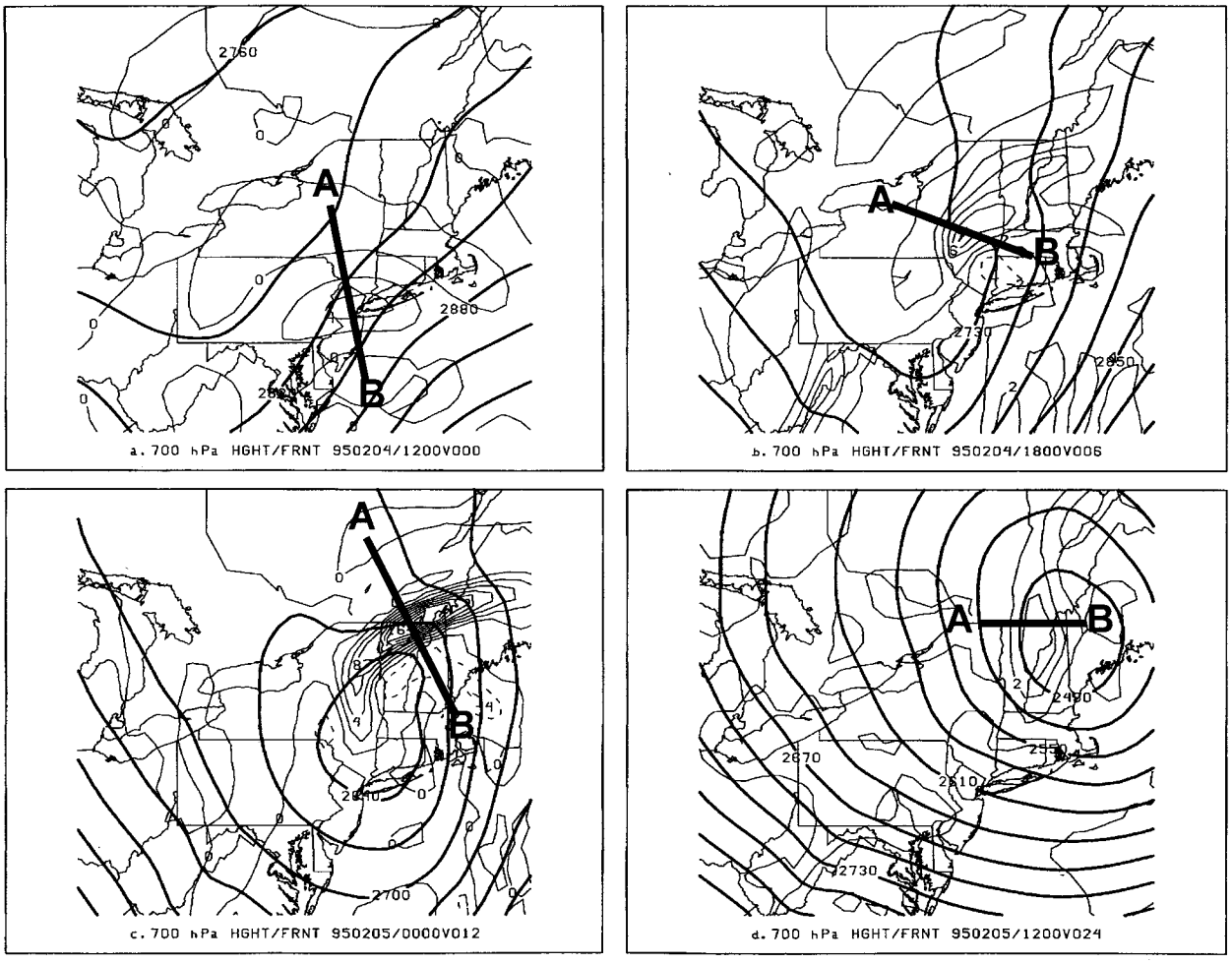

FIG. 4. The Meso Eta forecast 700-hPa geopotential heights and frontogenetic function for (a) 0-h forecast valid 1200 UTC 4 Feb 1995, (b) 6-h forecast valid 1800 UTC 4 Feb 1995, (c) 12-h forecast valid 0000 UTC 5 Feb 1995, and (d) 24-h forecast valid 1200 UTC 5 Feb 1995. Shown are the 700-hPa heights (heavy contours, 30-m interval) and 700-hPa frontogenetic function [light contours, contour interval 2 K (100 km)$^{-1}$ (3 h)$^{-1}$]. Positive values (solid) denote regions of frontogenesis, negative values (dashed) denote regions of frontolysis.

cycle. A negatively tilted 300-hPa trough axis was positioned from Lower Michigan southeast across the Ohio Valley to off the South Carolina coast at 14/1800 UTC (Fig. 7a). The 300-hPa trough moved northeast and became a closed upper-level low over Virginia and Maryland between 14/1800 UTC and 15/0900 UTC (Figs. 7b and 7c). The upper-level low remained nearly stationary through 15/1200 UTC (Fig. 7d). The 1000-hPa low moved from off the North Carolina coast to eastern Pennsylvania during this time period becoming an extensive cyclone. The distance between the 300-hPa trough axis and 1000-hPa low was decreasing during this time period indicative of cyclogenesis. After 15/0900 UTC, the cyclone had a nearly vertical structure with the low-level cyclone close to the upper-air low (Figs. 7c and 7d).

The central Pennsylvania (KCCX) WSR-88D base reflectivity is shown at 15/0301 UTC, which was near the height of the heavy snowfall in Pennsylvania (Fig. 8). Similar to the previous case, a distinct mesoscale snowband was located near the northwest edge of the precipitation shield in north-central Pennsylvania. This mesoscale snowband developed over north-central Pennsylvania between 14/2100 UTC and 15/0000 UTC and slowly propagated to the west. The mesoscale snowband eventually rotated counterclockwise and achieved a more north-to-south orientation by the time it weakened across southwest New York State and northwest Pennsylvania. The slow movement of this mesoscale snowband explained the local storm total snowfall maximum in north-central Pennsylvania (Fig. 6). The other snowfall maximum in southwest Pennsylvania was associated with previous mesoscale snowbands and orographic lift.

Figure 9 shows the Meso Eta 14/1500 UTC forecast cycle 03–18-h forecast of the 700-hPa geopotential height and frontogenetic function. Initially, a 700-hPa trough existed across the middle Atlantic states with a

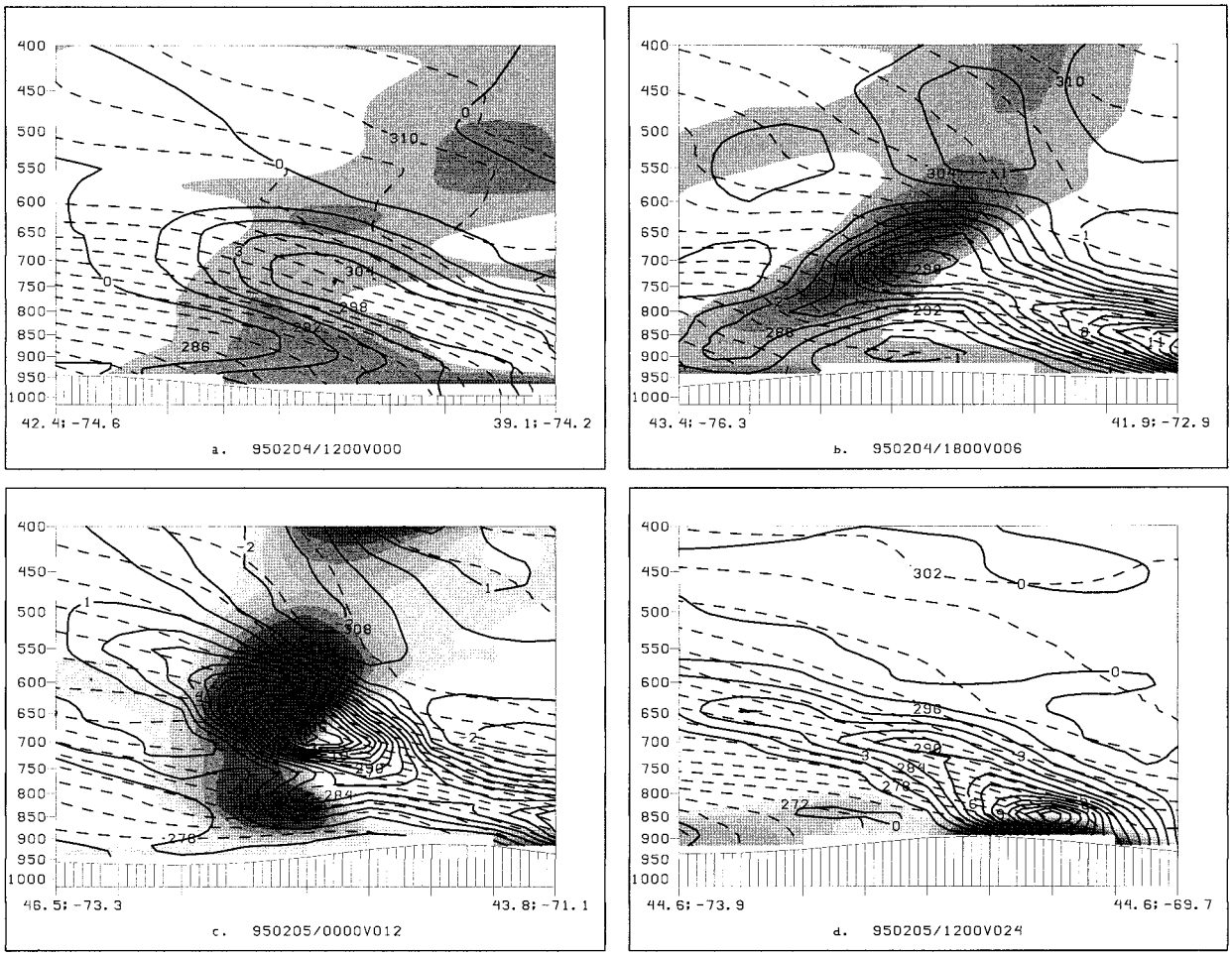

FIG. 5. Meso Eta Model forecast cross sections depicting the frontogenetic function [heavy contours, contour interval 1 K (100 km)$^{-1}$ (3 h)$^{-1}$], saturation equivalent potential temperature (dashed, contour interval 2 K), and equivalent potential vorticity [negative values shaded, shading interval of 3×10^{-7} K (Pa s)$^{-1}$, darkest shades represent the most negative values] (a) 0-h forecast valid 1200 UTC 4 Feb 1995, (b) 6-h forecast valid 1800 UTC 4 Feb 1995, (c) 12-h forecast valid 0000 UTC 5 Feb 1995, and (d) 24-h forecast valid 1200 UTC 5 Feb 1995. The cross-section endpoints are depicted in Fig. 4 for the corresponding forecast times where ''A'' is the left endpoint and ''B'' is the right endpoint.

weak area of frontogenesis present in Pennsylvania to the northwest of the 1000-hPa low (Fig. 9a). As the 700-hPa low emerged from the trough, the band of frontogenesis intensified and remained northwest of the 700-hPa low (Fig. 9b). The frontogenesis was strongest at this stage, and likewise, the mesoscale snowband reached its greatest intensity near 15/0300 UTC (see Fig. 8). Similar to the previous case, the mesoscale snowband was closely correlated to the 700-hPa frontogenesis maximum (cf. Figs. 8 and 9b). Eventually, the band of frontogenesis weakened as it remained to the northwest of the 700-hPa low (Fig. 9c). It was at this time that the 1000-hPa low was almost directly underneath the middle- and upper-level lows.

The frontogenesis, EPV, and θ_{es} cross sections reveal that, initially, a deep layer of negative EPV was present in conjunction with the weak area of frontogenesis (Fig. 10a). The negative EPV extended almost the entire depth of the troposphere and was entirely associated with CSI. By 15/0300 UTC, an intense, isolated maximum in frontogenesis emerged near 700 hPa with the development of the 700-hPa low (Fig. 10b). The EPV became highly negative at this time directly above the midlevel frontogenesis maximum. The mesoscale snowband reached its greatest intensity at this time as well. The negative EPV was entirely associated with CSI in the vicinity of the mesoscale snowband and region of intense midlevel frontogenesis. There was a small region of CI displaced well to the warm side of the frontogenesis maximum and mesoscale snowband (Fig. 10b). The release of CI may explain the heavier precipitation seen on radar to the east of the mesoscale snowband in the Susquehanna Valley of central Pennsylvania (Fig. 8). Finally, as the 1000-hPa low and middle- to upper-level lows became nearly collocated, the EPV became positive in conjunction with a much weaker region of

FIG. 6. Same as Fig. 1 except for 14 and 15 Nov 1995 over Pennsylvania and adjacent states.

frontogenesis in the model fields (Fig. 10c), similar to the previous case. At the same time, WSR-88D base reflectivity data (not shown) showed a marked decrease in the snowfall intensity and the mesoscale snowband subsequently disappeared.

This case also exhibited a *synergistic relationship* between frontogenesis and EPV in the Meso Eta Model forecasts. The 12-h forecast Meso Eta Model fields indicated that an intense region of frontogenesis would develop nearly coincident to a region of highly negative EPV over north-central Pennsylvania, where the mesoscale snowband formation became most prominent. Again, this illustrates the usefulness of mesoscale model frontogenesis and EPV fields for inferring potential mesoscale band formation and heavy snowfall in the short term.

c. The 12 January 1996 northeastern U.S. snowstorm

On 12 January 1996, a narrow band of very heavy snow fell across northeastern Pennsylvania and southern

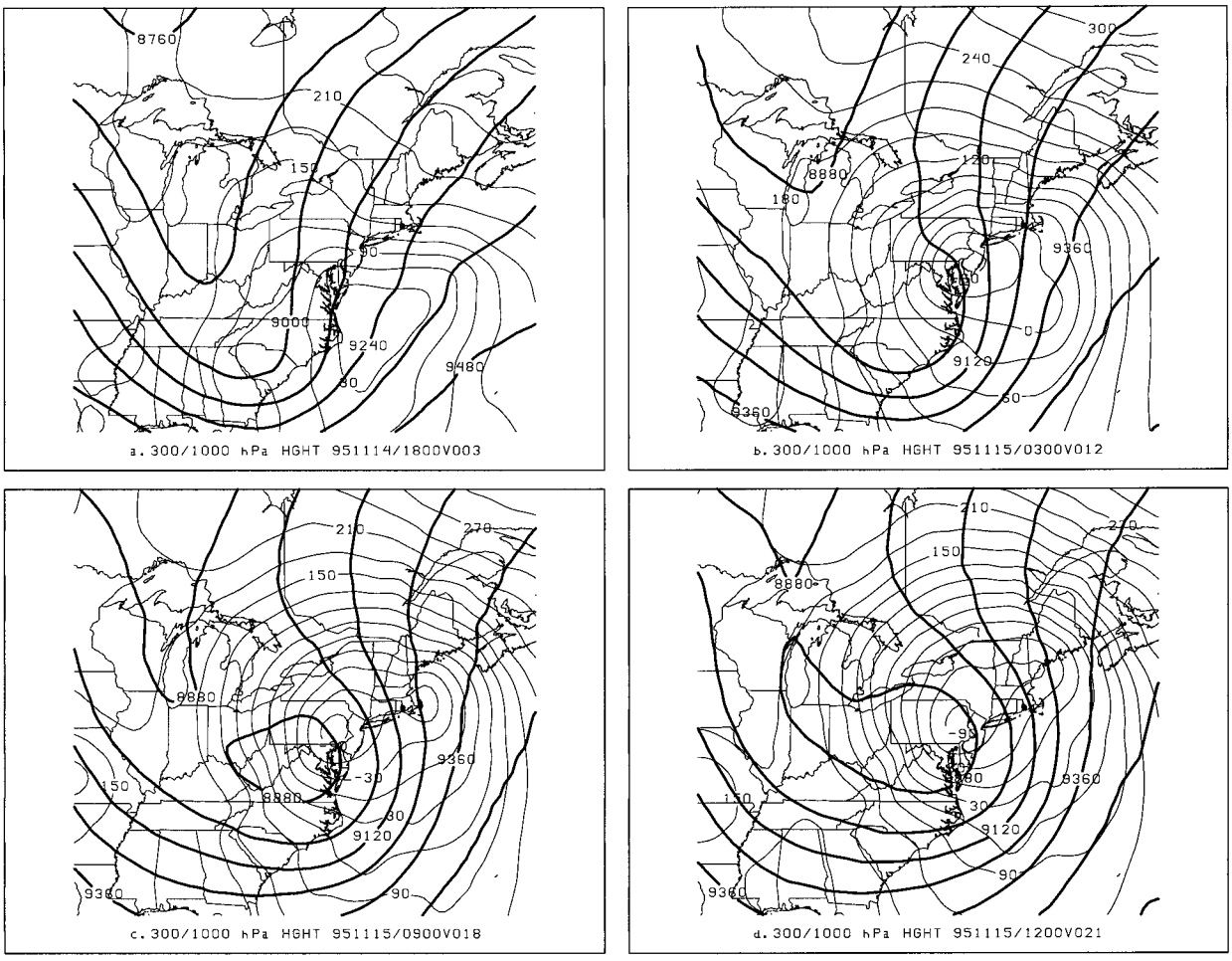

FIG. 7. Same as Fig. 2 except for (a) 3-h forecast valid 1800 UTC 14 Nov 1995, (b) 12-h forecast valid 0300 UTC 15 Nov 1995, (c) 18-h forecast valid 0900 UTC 15 Nov 1995, and (d) 21-h forecast valid 1200 UTC 15 Nov 1995.

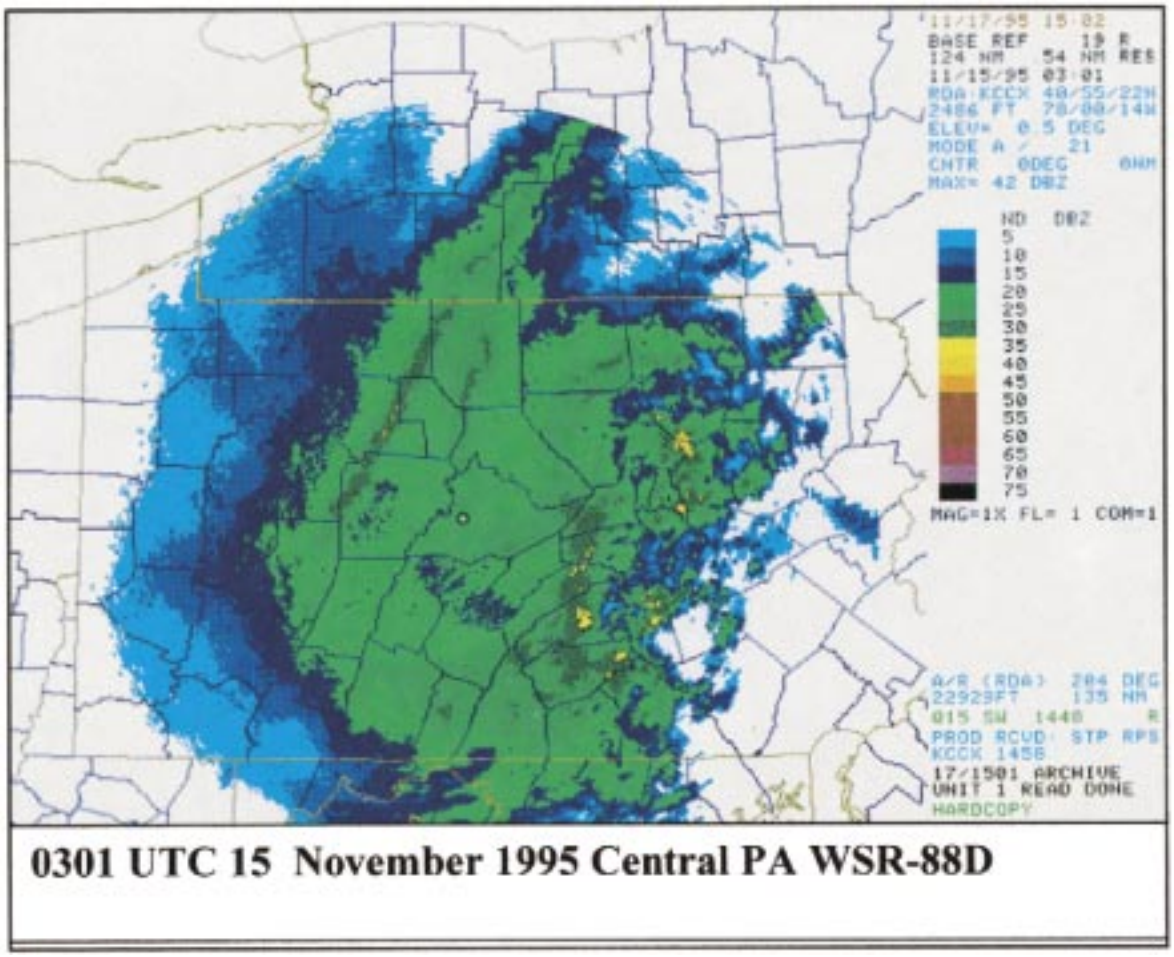

FIG. 8. Same as Fig. 3 except for the KCCX WSR-88D and at 0301 UTC 15 Nov 1995.

New York State (Fig. 11). Total snowfall surpassed 60 cm (24 in.) in extreme northeastern Pennsylvania with an extremely sharp cutoff to the storm total snowfall over north-central Pennsylvania and the Finger Lakes region of New York State. Figure 12 shows the 300- and 1000-hPa geopotential heights as depicted by the 12/1500 UTC Meso Eta forecast cycle. A 300-hPa trough was positioned over West Virginia at 12/1800 UTC (Fig 12a). The 300-hPa trough moved to eastern Pennsylvania and New Jersey by 13/0300 UTC (Figs. 12b–d). The 1000-hPa low moved from the Delaware coast to Long Island between 12/1800 UTC and 13/0300 UTC (Fig. 12). Unlike the previous two cases, the distance between the 300-hPa trough axis and 1000-hPa low did not decrease significantly and the 1000-hPa low deepened only slightly. Eventually, this cyclone weakened in an upper-level confluent zone over the Canadian Maritimes.

Figure 13 shows the WSR-88D base reflectivity data from KBGM. Two mesoscale bands of heavy snowfall were present in close proximity to each other over northeastern Pennsylvania and south-central New York state by 12/2140 UTC. These mesoscale snowbands merged over northeast Pennsylvania and south-central New York into one main band and possessed extraordinary snowfall rates. A spotter in Susquehanna County, Pennsylvania, underneath one of these bands, reported 15 cm (6 in.) *in one hour*. The mesoscale snowband(s) moved northeast parallel to its orientation resulting in a swath of very heavy snowfall in a narrow band from northeast Pennsylvania through eastern New York State (Fig. 11). Again, similar to the previous two cases, there was a very sharp cutoff to the heavy snowfall to the north and west.

The mesoscale snowband formed to the left of the Meso Eta 700-hPa low track (Fig. 14), which allowed it to remain nearly stationary relative to the movement of the system. Unlike the previous two cases, this snowstorm did not progress through all the stages of cyclogenesis. The low-level cyclone did not become collocated with the middle- to upper-air troughs (Fig. 12). The 700-hPa low intensified between 12/1800 UTC and about 13/0000 UTC (Figs. 14a and 14b). After 13/0000 UTC, the 700-hPa low weakened and became a trough

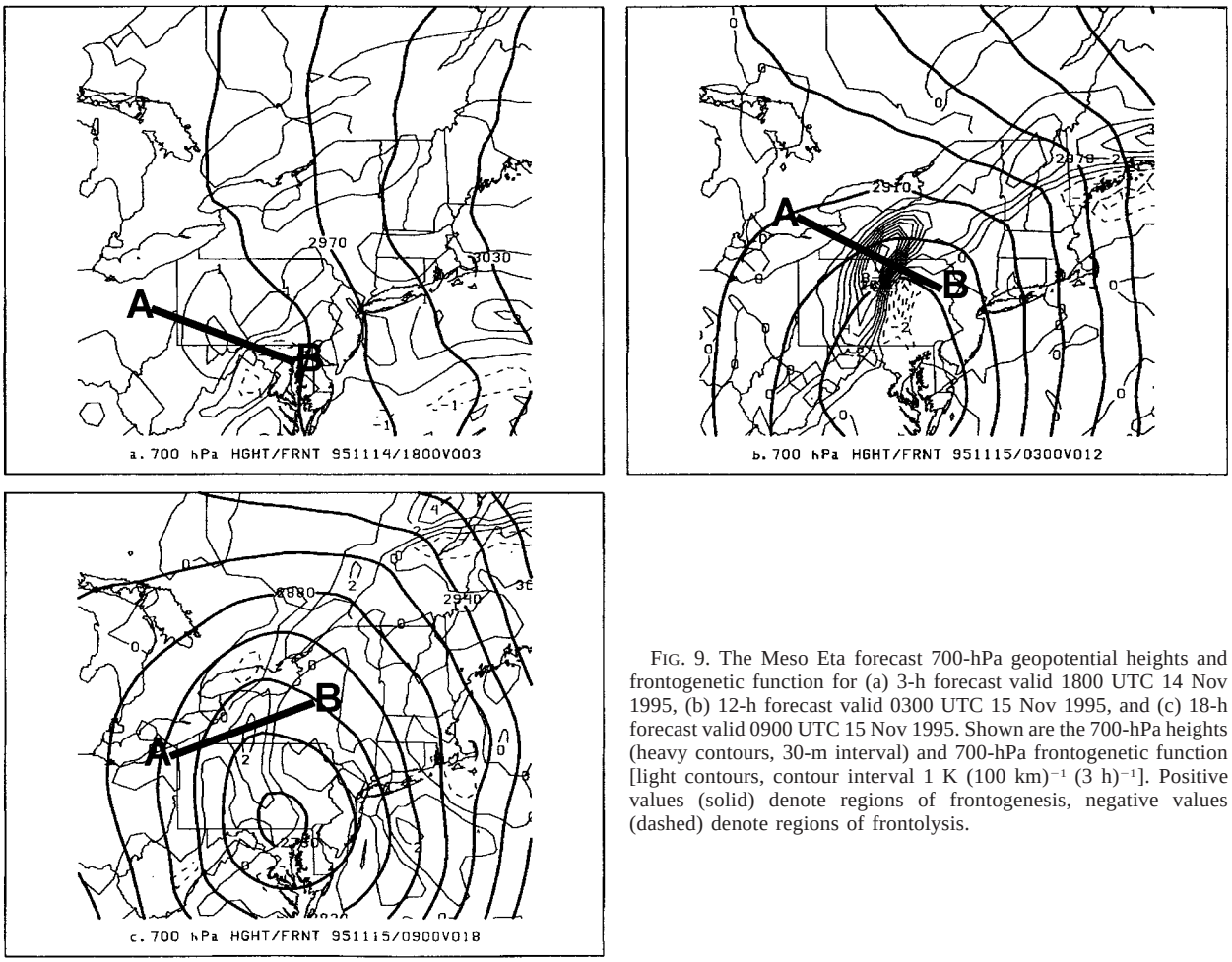

FIG. 9. The Meso Eta forecast 700-hPa geopotential heights and frontogenetic function for (a) 3-h forecast valid 1800 UTC 14 Nov 1995, (b) 12-h forecast valid 0300 UTC 15 Nov 1995, and (c) 18-h forecast valid 0900 UTC 15 Nov 1995. Shown are the 700-hPa heights (heavy contours, 30-m interval) and 700-hPa frontogenetic function [light contours, contour interval 1 K (100 km)$^{-1}$ (3 h)$^{-1}$]. Positive values (solid) denote regions of frontogenesis, negative values (dashed) denote regions of frontolysis.

(Fig. 14c). Eventually, the entire short-wave feature weakened in the upstream upper-level confluent zone. Similar to the previous cases, a band of 700-hPa frontogenesis emerged and intensified to the northwest of the 1000-hPa low (Figs. 12a and 12b) with the development of the 700-hPa low (Figs. 14a and 14b). The frontogenesis band at 700 hPa, again, closely correlated to the mesoscale snowband(s) on radar (cf. Figs. 13 and 14b). The band of frontogenesis at 700 hPa eventually weakened and moved to a position northeast of the 700-hPa trough (Figs. 14c and 14d).

Like the previous cases, a large area of negative EPV initially was present in conjunction with a region of frontogenesis (Fig. 15a). The negative EPV was initially associated with CSI. An intense maximum in frontogenesis developed near 700 hPa between 12/1800 UTC and 13/0300 UTC at the same time that the EPV became highly negative (Figs. 15b and 15c). Similar to the previous two cases, the frontogenesis became *stronger* at midlevels as the EPV became *highly negative*. Again, the mesoscale snowbands in northeast Pennsylvania and upstate New York reached their maximum intensity at this time. At 12/2100 UTC, there was a layer of CI present above the frontogenesis region within the larger region of CSI (Fig. 15b). This suggests that the release of CI, in conjunction with CSI, may have been a factor in forming the multiple mesoscale snowbands seen in Fig. 13, which was close to this model time period. Multiple band formation is possible when CI is present in conjunction with CSI since CI favors more vertical updrafts. This, in turn, may allow for more updrafts to fit within a region of frontogenetical forcing and lead to multiple band formation. It is important to note that this is not a necessary condition for multiple mesoscale band formation, since there is evidence that CSI alone can produce multiple mesoscale snowbands (Reuter and Yau 1990; Snook 1992; Grumm and Nicosia 1997).

By 13/0300 UTC, as the EPV attained the most negative values, the CI was gone with CSI entirely present. It is interesting to point out that the multiple snowbands merged into one main snowband over eastern New York by this time. By 13/0900 UTC, the EPV increased significantly in conjunction with a weaker region of frontogenesis (Fig. 15d), similar to the other cases.

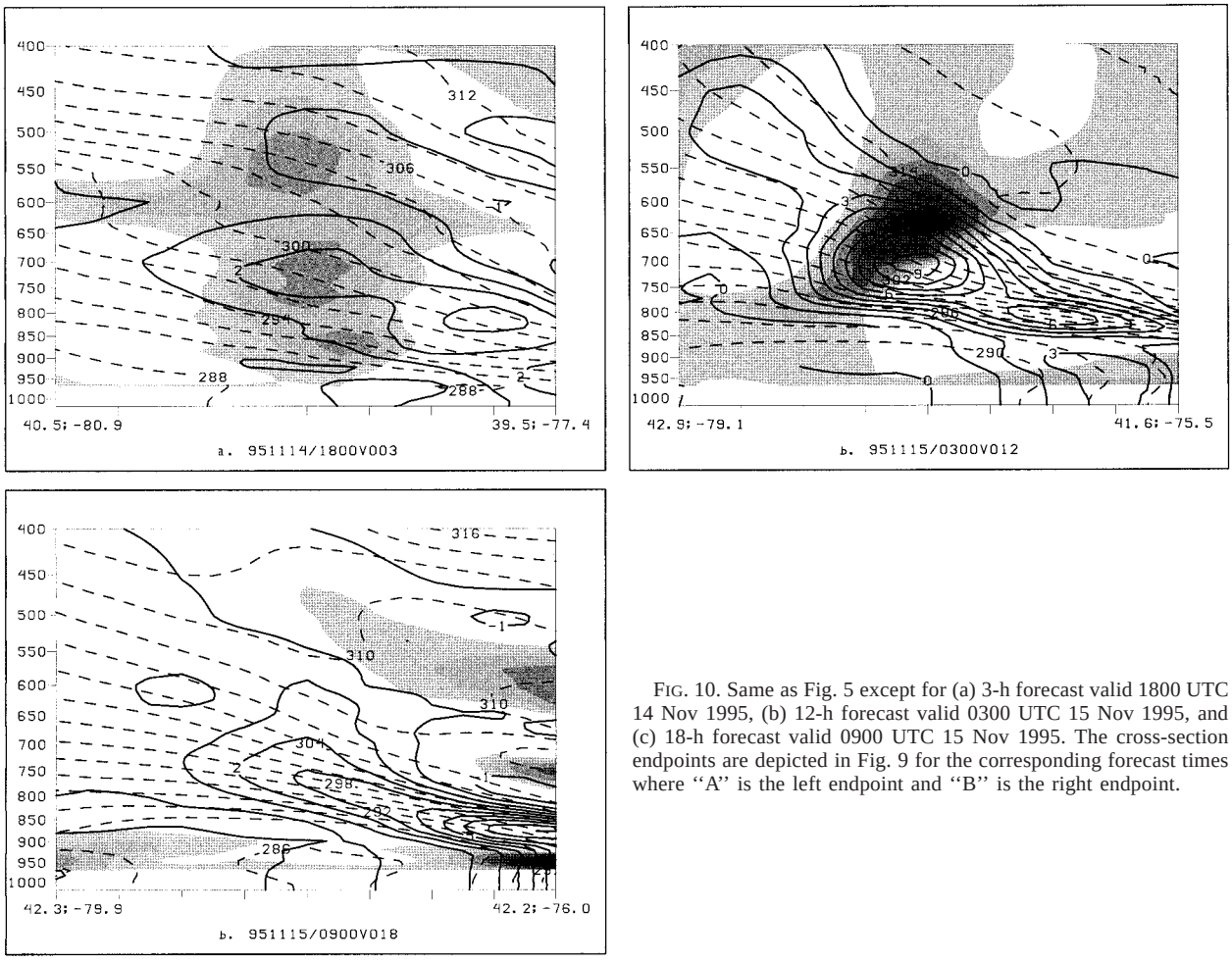

FIG. 10. Same as Fig. 5 except for (a) 3-h forecast valid 1800 UTC 14 Nov 1995, (b) 12-h forecast valid 0300 UTC 15 Nov 1995, and (c) 18-h forecast valid 0900 UTC 15 Nov 1995. The cross-section endpoints are depicted in Fig. 9 for the corresponding forecast times where ''A'' is the left endpoint and ''B'' is the right endpoint.

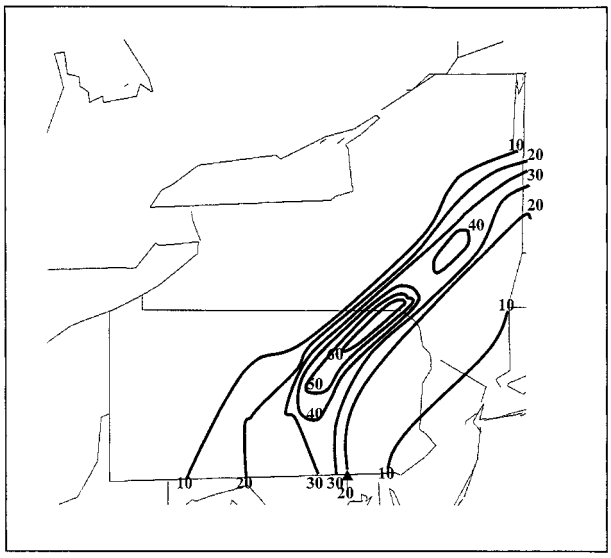

FIG. 11. Same as Fig. 1 except for 12 and 13 Jan 1996 over Pennsylvania and adjacent states.

This case illustrates that major cyclogenesis does *not* have to be present for very heavy snowfall to occur. The development of negative EPV in association with midlevel frontogenesis appears to be an important signature for forecasting heavy snowfall even for cyclones of a weaker magnitude. The Meso Eta Model frontogenesis and EPV fields showed the development of a deep layer of negative EPV in association with an intensifying midlevel frontogenesis maximum close to where the heaviest snow fell. Additionally, the presence of CI, in addition to CSI, may be an important factor for anticipating heavy snowfall regardless of the intensity of the extratropical cyclone.

d. Summary of cases

Each case exhibited a narrow mesoscale snowband(s) close to the north edge of the precipitation shield that closely correlated to a band of frontogenesis at 700 hPa and a region of highly negative EPV as depicted by the Meso Eta Model. The band of frontogenesis formed to the north of the developing 700-hPa low. Meso Eta

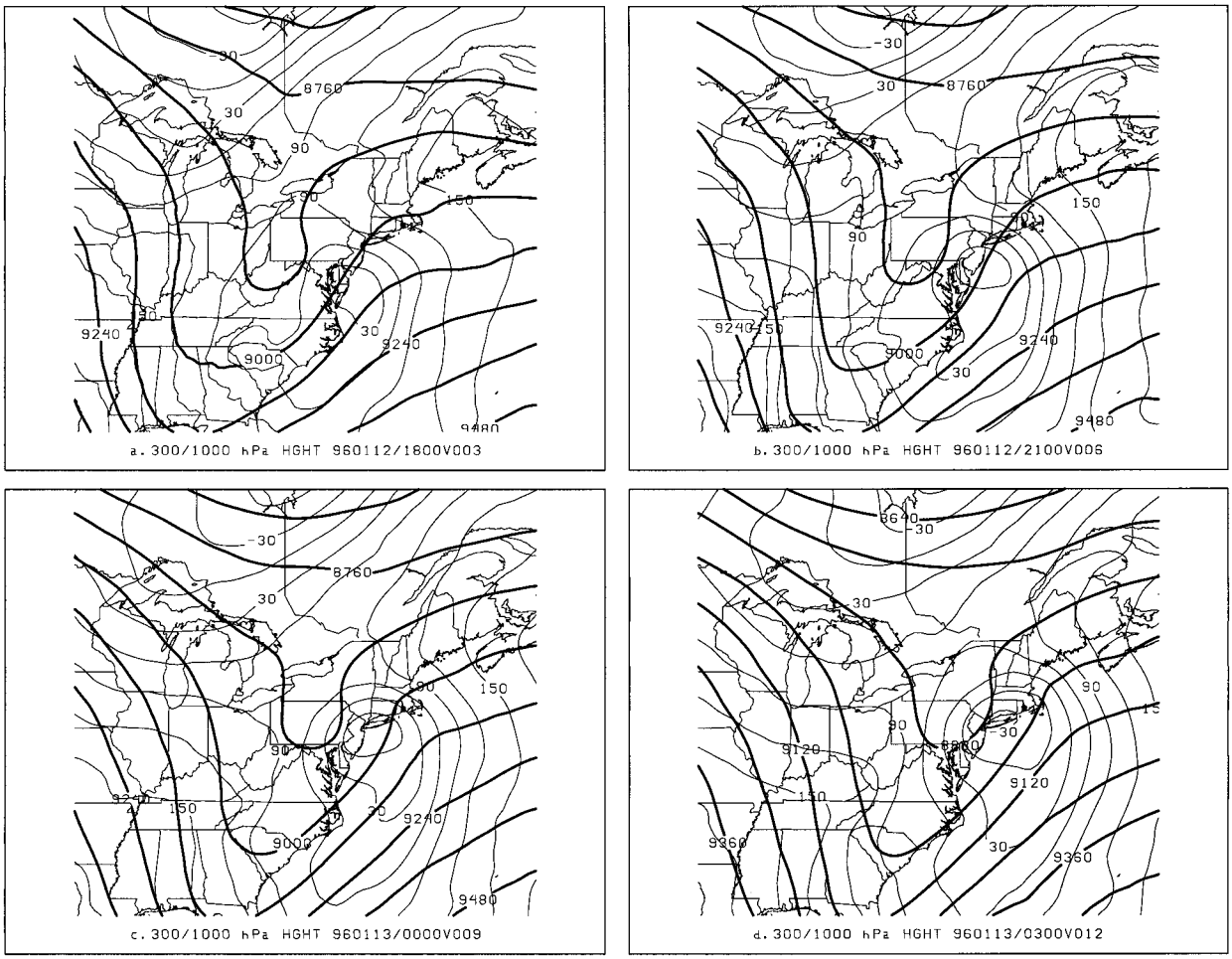

FIG. 12. Same as Fig. 2 except for (a) 3-h forecast valid 1800 UTC 12 Jan 1996, (b) 6-h forecast valid 2100 UTC 12 Jan 1996, (c) 9-h forecast valid 0000 UTC 13 Jan 1996, and (d) 12-h forecast valid 0300 UTC 13 Jan 1996.

Model cross-sectional analyses revealed that an isolated maximum in frontogenesis formed near 700 hPa, in each case, just below a region of highly negative EPV. The mesoscale snowbands produced large snowfall rates and were a main factor in the heaviest storm total snowfall. In addition, all three snowstorms possessed a relatively sharp cutoff in storm total snowfall to the north and west of the maximum snowfall.

Cross-sectional analyses indicated that a synergistic relationship between frontogenesis and EPV was evident for each case. The frontogenesis intensified and became an isolated maximum near 700 hPa at the same time that the EPV decreased sharply. Eventually, the maximum in frontogenesis in the midtroposphere was present directly underneath the region of the most negative EPV. This occurred near the time of maximum mesoscale snowband formation. In each case, the frontogenesis and negative EPV intensified with the development of the midlevel low. This synergy between frontogenesis and negative EPV and the subsequent formation of long-lasting mesoscale snowbands is consistent with the results of Xu (1989). Xu (1989) showed, theoretically, that frontogenesis in the presence of negative EPV produces long-lasting mesoscale precipitation bands. He postulated that CSI alone, without frontogenetic forcing, produced short-lived banded precipitation structures. The frontogenesis appeared to be an important factor for the maintainence of the precipitation bands and continual release of CSI.

Eventually, the EPV increased significantly with each case becoming largely positive close to a region of weakening frontogenesis. This was especially true for the February and November cases in which the EPV became positive over most of the troposphere to the west of the cyclone center. It is interesting to note that these two cases exhibited low-level cyclones that became collocated with the middle- and upper-level lows at this time.

Examination of model θ_{es} conjunction with EPV revealed that the negative EPV with each case was almost entirely CSI. At times, there were much smaller regions of CI present on the warm side of the frontogenesis

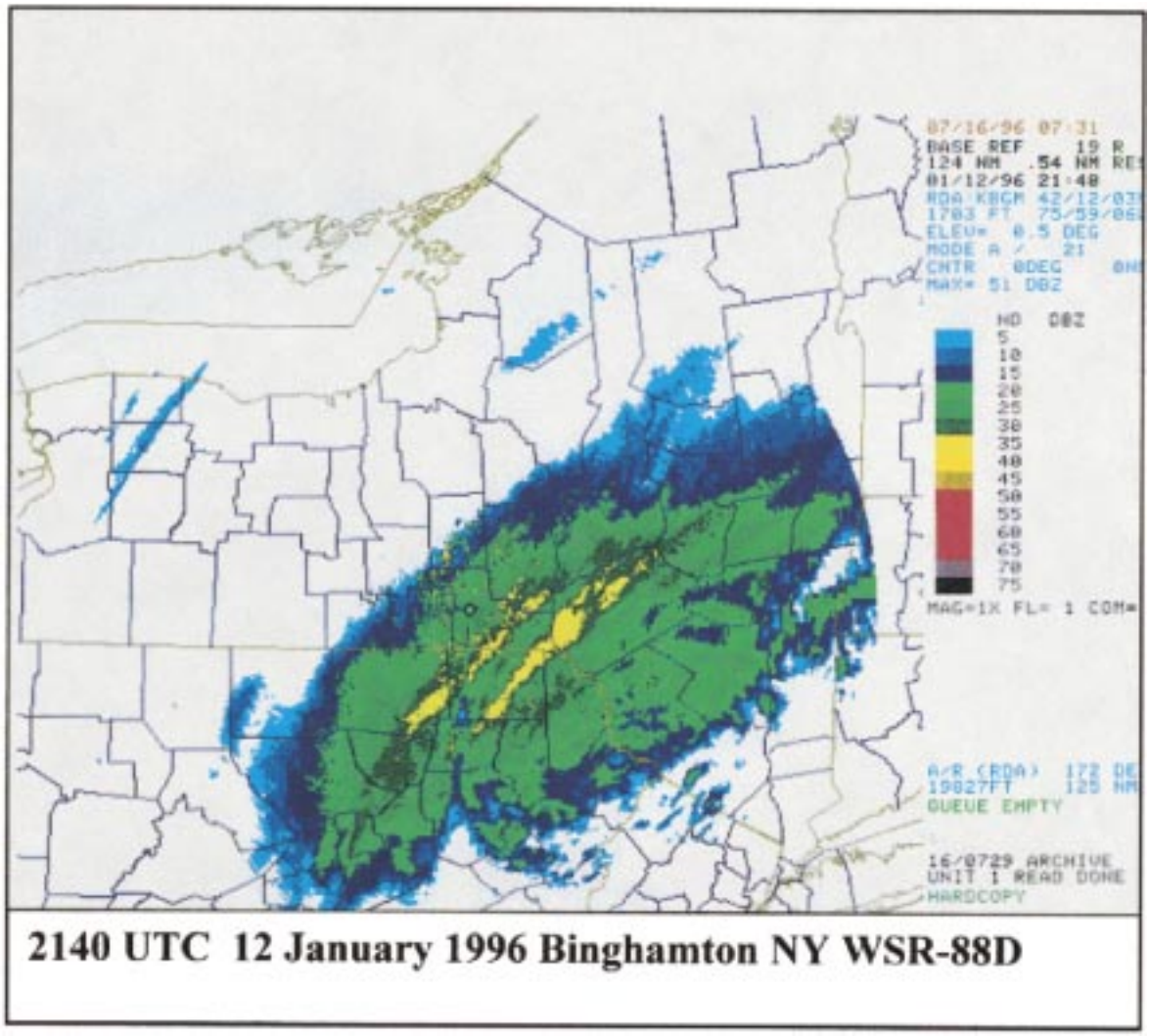

FIG. 13. Same as Fig. 3 except for the KBGM WSR-88D base reflectivity at 2140 UTC 12 Jan 1996.

region in each case. The CI was embedded within larger regions of CSI, initially, before the frontogenesis reached its maximum intensity and the EPV reached its most negative values. For each case, the CI was short lived and did not last for more than one model forecast time period.

Unlike the other two cases, the radar imagery for the January case (Fig. 13) corresponded to the model forecast time when the Meso Eta possessed CI, in addition to CSI (Fig. 15b). For the other two cases, the radar imagery (Figs. 3 and 8) corresponded to the model forecast times when CSI was almost entirely present (Figs. 5b and 10b). Unlike the other cases, the January case possessed two mesoscale snowbands while the other cases had single mesoscale snowbands (during the time periods corresponding to the radar imagery). In addition, snowfall rates and storm total snowfall from the January case exceeded the other two cases. The CI disappeared in the model fields in the January case by the next model forecast time (three forecast hours after the valid forecast time in Fig. 15b). Consequently, radar observations indicated that the multiple nature of the snowbands disappeared (not shown) and a single mesoscale snowband became dominate over eastern New York State. The storm total snowfall (Fig. 11) for the January case indicates that the heaviest snowfall occurred over extreme northeast Pennsylvania where the Meso Eta possessed this layer of CI. Thus, it is possible that the release of CI, in addition to CSI, favored heavier snowfall rates in the January case when compared to the release of CSI alone in the other two cases.

The February and November cases also possessed stronger frontogenesis than the January case during the times corresponding to the radar imagery. Since single mesoscale snowbands were observed in these two cases, this suggests that frontogenetic forcing could have been solely responsible for the mesoscale snowbands at these time periods (Snook 1992). However, based on the me-

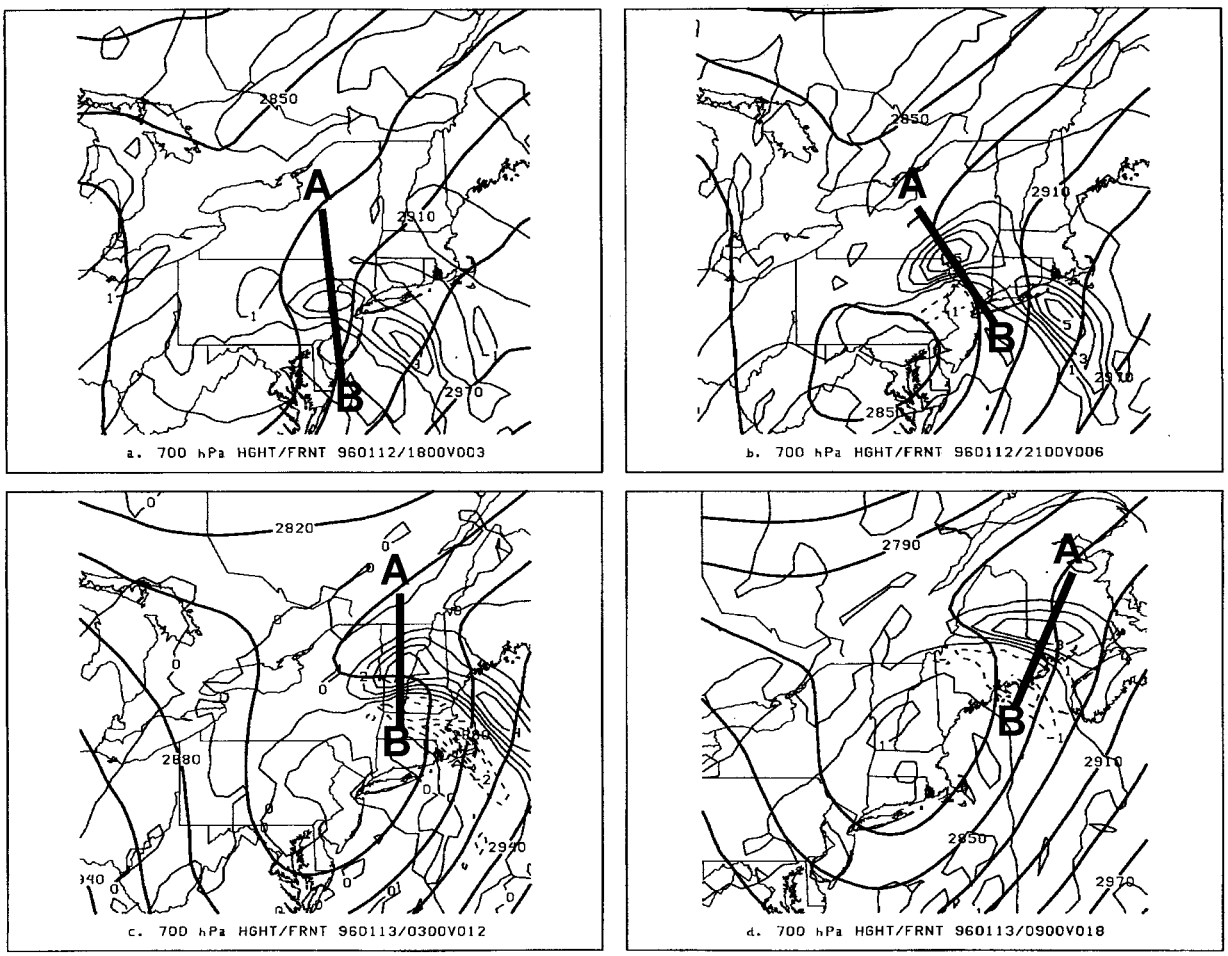

FIG. 14. Same as Fig. 9 except for (a) 3-h forecast valid 1800 UTC 12 Jan 1996, (b) 6-h forecast valid 2100 UTC 12 Jan 1996, (c) 12-h forecast valid 0300 UTC 13 Jan 1996, and (d) 18-h forecast valid 0900 UTC 13 Jan 1996.

soscale model data, it is more likely that both CSI and frontogenetic forcing were responsible for the mesoscale snowbands in these cases for the following reasons: 1) a deep layer of negative EPV, which was entirely CSI, was present close to the maximum region of frontogenesis; 2) saturation existed; and 3) vertical motion was present. Thus, the frontogenetic forcing provided the lifting mechanism that led to saturation and the eventual release of the CSI.

All three cases illustrate that forecasting the presence of mesoscale snowbands and attendant heavy snowfall is possible operationally. Using model gridded data, forecasters should look for frontogenetic regions between 850 and 500 mb to the north of a developing surface low. Cross sections of EPV and θ_{es} should be taken perpendicular to the isotherms and across the strongest region of frontogenesis. If the EPV is highly negative close to a region of frontogenesis and saturation exists, forecasters can anticipate the potential for heavy snowfall in this region. In addition, if the θ_{es} surfaces decrease with height on the warm side of the frontogenesis region, CI could be released, which might lead to heavier snowfall rates. Where the θ_{es} increases with height in a negative EPV region, forecasters can anticipate CSI mesoscale snowbands if vertical motion and saturation are present. Use of a finer-resolution mesoscale model is preferred since mesoscale models can simulate frontogenetic forcing on a more realistic scale than coarser-resolution synoptic-scale models.

4. Discussion

a. Frontogenesis and the reduction of equivalent potential vorticity

Since each case possessed a highly negative region of EPV, it is apparent that there was a significant reduction in EPV north of each low-level cyclone. This reduction in EPV occurred close to the frontogenetic region with highly negative values becoming present near the time the midlevel low center emerged. The cross-product factor in (3), that is, $k \cdot (\nabla\theta_e \times \nabla\theta)$, was calculated at 500 hPa (Fig. 16) to estimate the generation of EPV in the midlevels, where the highest negative

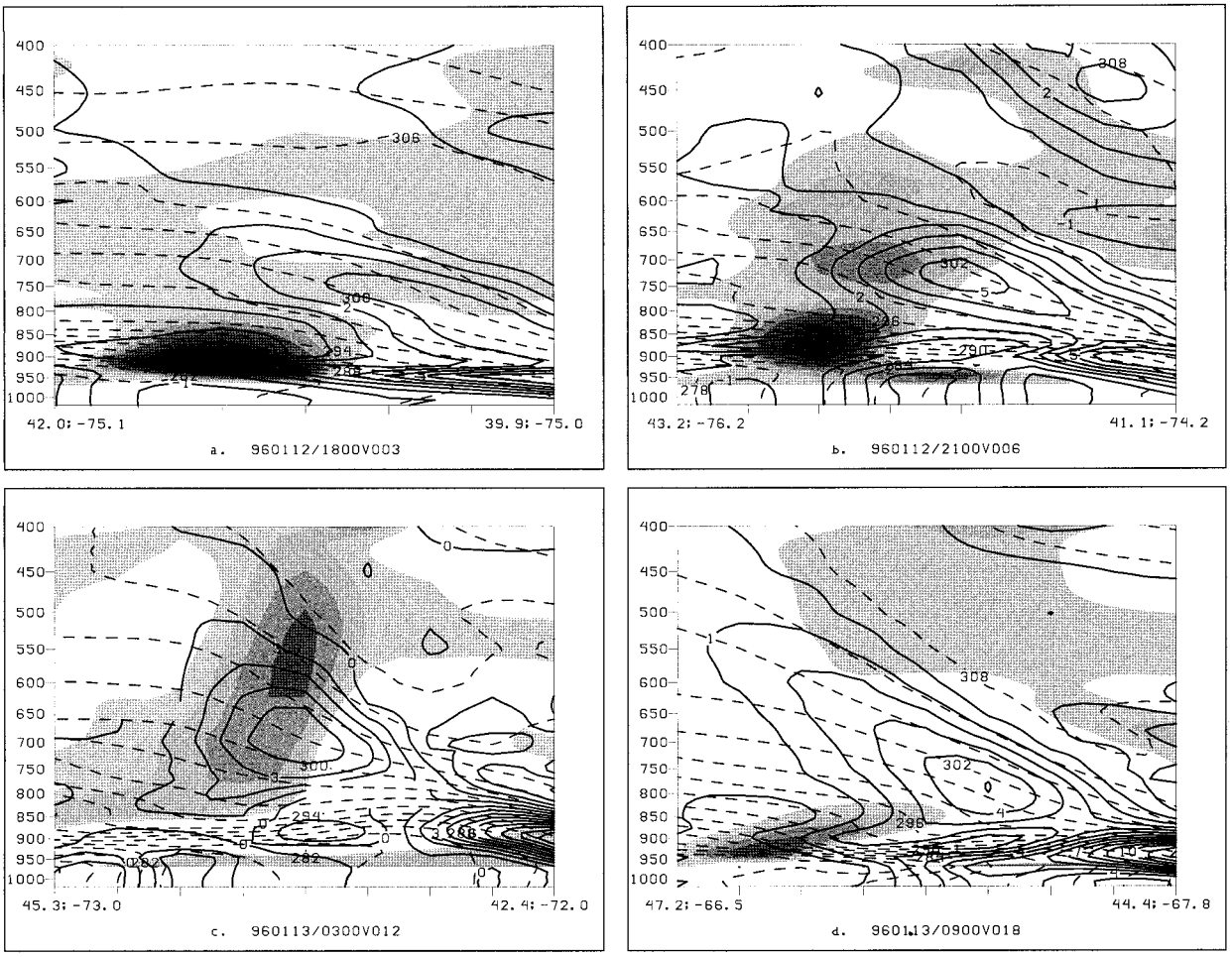

FIG. 15. Same as Fig. 5 except for (a) 3-h forecast valid 1800 UTC 12 Jan 1996, (b) 6-h forecast valid 2100 UTC 12 Jan 1996, (c) 12-h forecast valid 0300 UTC 13 Jan 1996, and (d) 18-h forecast valid 0900 UTC 13 Jan 1996. The cross-section endpoints are depicted in Fig. 14 for the corresponding forecast times where "A" is the left endpoint and "B" is the right endpoint.

values of EPV were found. The time periods for each case in Fig. 16 were chosen corresponding to the height of mesoscale band formation as depicted in Figs. 3, 8, and 13. These time periods also correspond to the time when strong midlevel frontogenesis was present in conjunction with a region of highly negative EPV. It was found by performing a simple timescale analysis that the cross-product factor in (3) can reduce the EPV by 1.5×10^{-6} K (Pa s)$^{-1}$ (1.5 PVU) in about 12 h. This suggests that this term is a plausible source of negative EPV since the timescale of an extratropical cyclone undergoing cyclogenesis is on the order of a few days. This finding is also consistent with the conclusions of Bennetts and Hoskins (1979) and O'Hanley and Bosart (1989). The value of 1.5×10^{-6} K (Pa s)$^{-1}$ (1.5 PVU) was chosen for the timescale analysis since it was approximately the average maximum negative EPV value among the three cases. Values of the magnitude of the cross-product factor in (3) were chosen for the timescale analysis based on the average of the most negative values for each case seen in Fig. 16.

Figure 16 indicates that the generation term for EPV was significantly negative with each case, to the warm side of the midlevel frontogenetic regions. All three cases show that the generation term for EPV was highly negative close to the emerging dry tongue jet (Carlson 1980) at midlevels, which is depicted by the relative humidity and wind fields at 500 hPa (Fig. 16). For the February case (Fig. 16a) and the January case (Fig. 16c), the drying aloft was occurring on the warm side of, and adjacent to, the intense 700-hPa frontogenesis maxima seen in Figs. 4b and 14b, respectively. For the November case (Fig. 16b), the drying aloft (at this time period) was occurring well southeast of the intense midlevel frontogenesis and mesoscale snowband in north-central Pennsylvania. The November case was different from the other two cases in that it exhibited a more significant closed midlevel low circulation at this forecast time,

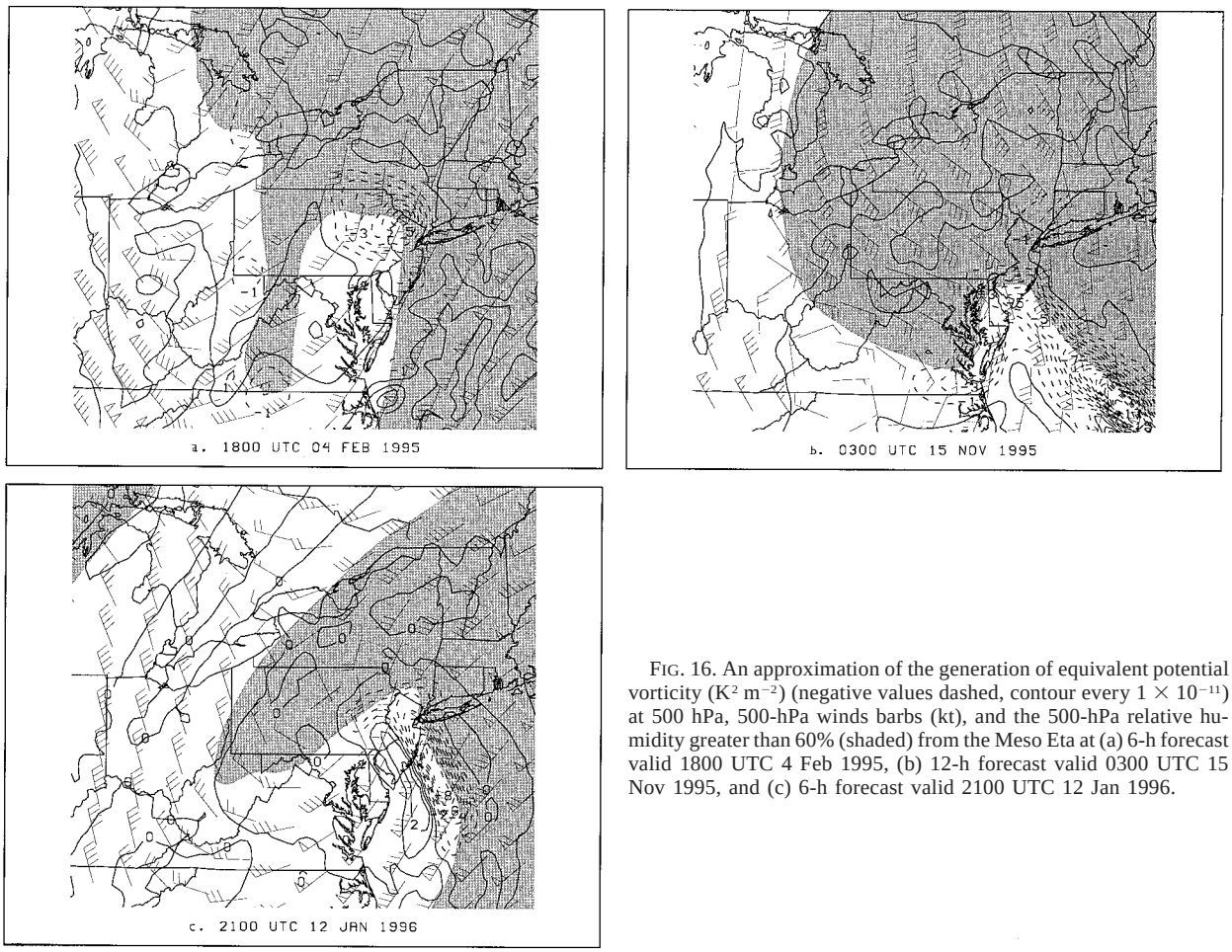

FIG. 16. An approximation of the generation of equivalent potential vorticity ($K^2\ m^{-2}$) (negative values dashed, contour every 1×10^{-11}) at 500 hPa, 500-hPa winds barbs (kt), and the 500-hPa relative humidity greater than 60% (shaded) from the Meso Eta at (a) 6-h forecast valid 1800 UTC 4 Feb 1995, (b) 12-h forecast valid 0300 UTC 15 Nov 1995, and (c) 6-h forecast valid 2100 UTC 12 Jan 1996.

with the mesoscale snowband diminishing markedly after the time period shown in Fig. 16b.[1] The other two cases did not possess significant midlevel low centers at the time periods displayed in Fig. 16 with the mesoscale snowbands remaining intense for another 6–12 more hours.

The reduction of EPV was associated with the ''zone'' where the midlevel dry tongue jet overlaid a low-level moist easterly jet streak, north of each surface low (not shown), and south of each midlevel frontogenesis maximum (Fig. 17). This low-level jet easterly streak is related to the formation of the cold conveyor belt (CCB) as discussed in Carlson (1980). It is this zone where differential moisture advection was most prevalent as midlevel drying occurred above the region dominated by the moisture-laden low-level easterly jet. The low-level easterly jet led to significant moisture advection in the model fields with each case below 500 hPa (not shown) and the region of midlevel drying. This is similar to the results in O'Handley and Bosart (1989) who found that the reduction of EPV was maximized near a midlevel dry intrusion during cyclogenesis.

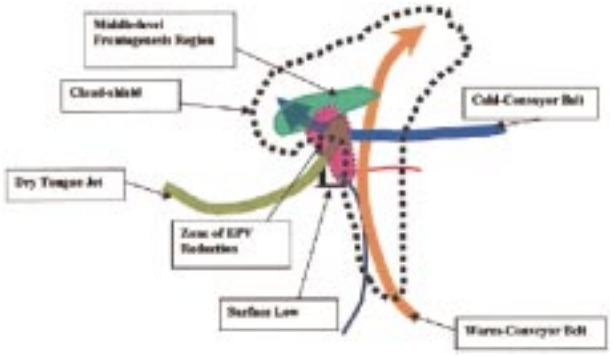

FIG. 17. Conceptual model depicting the frontogenesis region and zone of equivalent potential vorticity reduction within the context of the major components of a developing extratropical cyclone.

[1] Model grids for the time periods prior to the time period displayed in Fig. 16b were incomplete and the generation term estimated from (3) could not be calculated.

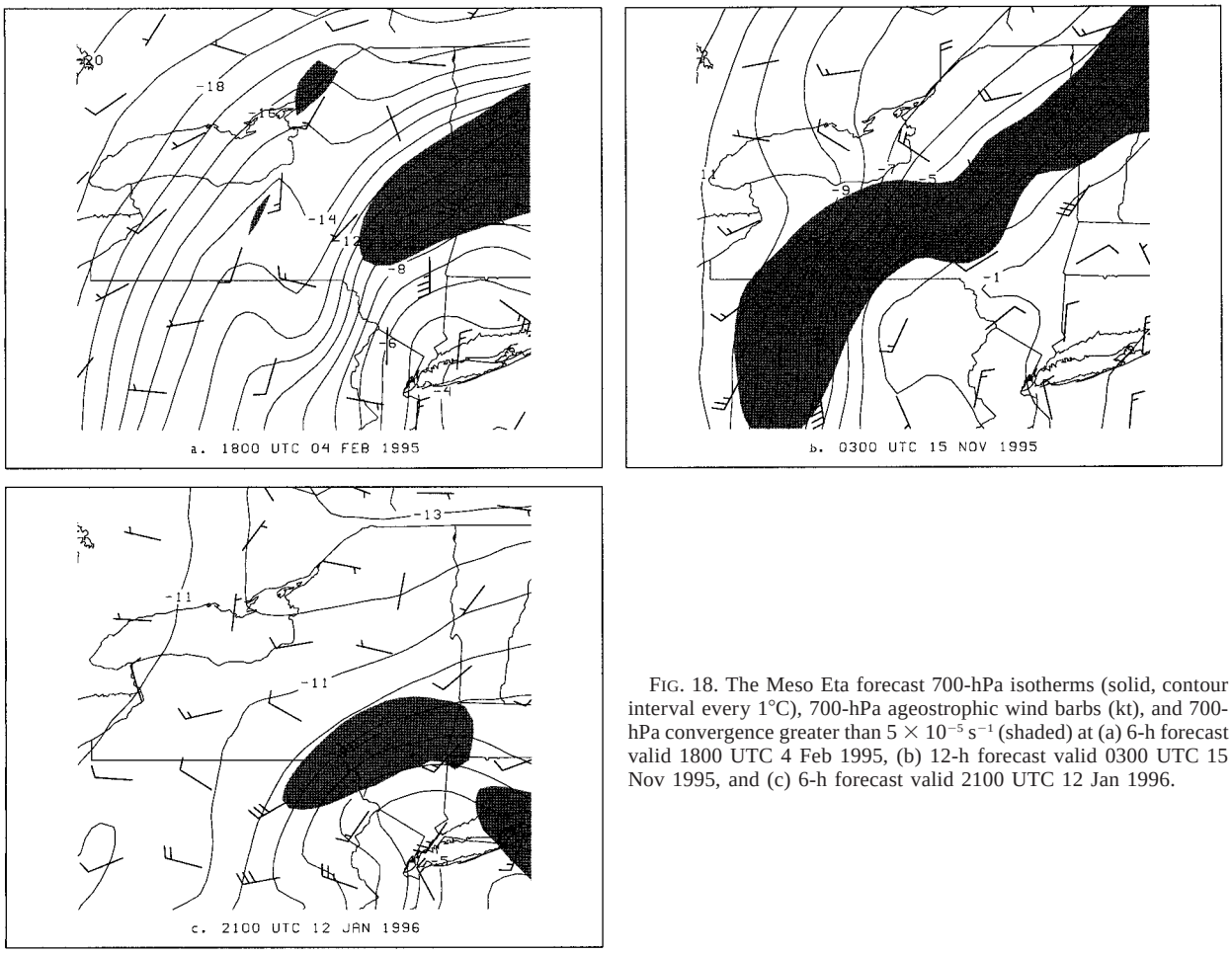

FIG. 18. The Meso Eta forecast 700-hPa isotherms (solid, contour interval every 1°C), 700-hPa ageostrophic wind barbs (kt), and 700-hPa convergence greater than 5×10^{-5} s^{-1} (shaded) at (a) 6-h forecast valid 1800 UTC 4 Feb 1995, (b) 12-h forecast valid 0300 UTC 15 Nov 1995, and (c) 6-h forecast valid 2100 UTC 12 Jan 1996.

Differential moisture advection leads to a steepening of the θ_e surfaces that is *independent* of the steepening of the θ surfaces that normally occurs from frontogenesis. The dry air advection aloft ensures that the atmosphere is not saturated in the middle to upper levels in this region. Since the M_g surfaces only adjust to changes in the steepness of the θ surfaces (to maintain thermal wind balance and preserved dry potential vorticity), EPV is lowered in the region where the dry air aloft overlays the moist low-level easterly flow (or CCB) near the warm advection zone. Eventually for each case, the EPV was reduced to a point in which it became negative, leading to CSI and, at times, smaller regions of CI. Since this region was characterized by large-scale ascent, CSI and, to a lesser extent, CI likely was released as the whole layer reached saturation.

Frontogenesis appeared to play an integral role in enhancing the differential moisture advection during cyclogenesis. By increasing the temperature gradient, frontogenesis supported an increase in the vertical shear to maintain thermal wind balance. Assuming the temperature gradient points to the south (colder air to the north), the change in vertical wind shear led to enhanced easterly flow in the low levels and enhanced westerly flow aloft. For each case, there was an increase in the easterly flow of the low levels that led to the development of an easterly low-level jet streak or CCB (not shown). This easterly low-level jet streak was a very important source of low-level moisture advection for each case. Conversely, the increase in westerly flow aloft was associated with strong midlevel dry advection and the arrival of the dry tongue jet aloft. Thus, by changing the vertical wind shear, frontogenesis supported an increase in the differential moisture advection and attendant reduction in EPV with each case. This process is quantified in (3). It is easy to see from (3) that, all else being equal, if the temperature gradient increases, EPV will be reduced.

All three cases possessed large temperature gradients at 700 hPa near the time when the midlevel frontogenesis was strong (Fig. 18). The February 1995 (Fig. 18a) and January 1996 cases (Fig. 18c) both displayed stronger temperature gradients in the same direction of the dry advection aloft in Figs. 16a and 16c, respectively. This indicates that the generation term for EPV may have become even more negative, in time, on the warm

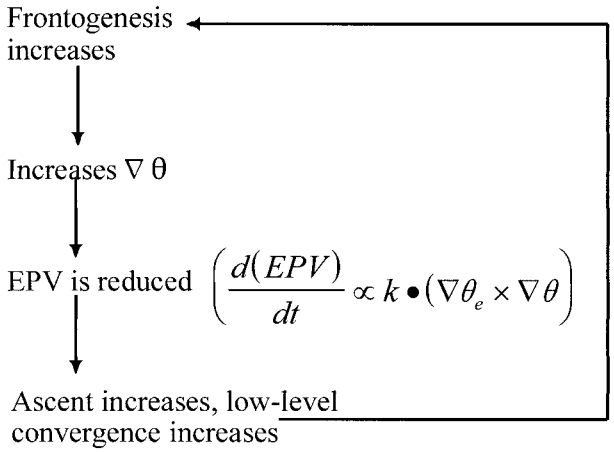

FIG. 19. Schematic depicting a proposed positive feedback mechanism between frontogenesis and the reduction of equivalent potential vorticity.

side of each frontogenesis maximum as each low-level cyclone tracked to the northeast.

b. Formation of the mesoscale snowbands

Once the warm side of the frontogenetic region (north of each surface low) became associated with lower EPV air, a positive feedback mechanism may have led to the formation of the long-lived mesoscale snowbands (Fig. 19). When low EPV is present with frontogenesis, stronger vertical motion results that becomes constricted to a smaller scale (Emanuel 1985). Stronger ascent parallel to the isotherms leads to stronger low-level convergence and upper-level divergence perpendicular to the isotherms. The convergence acts on the temperature gradient leading to stronger frontogenesis. All three cases showed strong convergence at 700 hPa coincident with the strongest 700-hPa frontogenesis supporting this argument (cf. Figs. 18, 4b, 9b and 14b). With stronger frontogenesis, the temperature gradient is increased (Fig. 18), which further reduces the EPV. This was evident in the February (Fig. 18a) and January (Fig. 18c) cases in which the frontogenesis maximum was still in the process of strengthening.

With the continual reduction in EPV, CSI and, to a lesser extent, CI developed in association with the frontogenetic regions. As air parcels ascended the isentropes in the warm air advection zone and reached saturation, CSI and, to a lesser extent, CI was released, resulting in enhanced vertical motion and mesoscale band formation. Furthermore, the release of CI and CSI in a region of frontogenesis leads to stronger vertical motion that is constricted to a smaller scale. The increase in vertical motion leads to an increase in low-level convergence, which in turn increases the frontogenesis. This further increases the temperature gradient, which further reduces the EPV by (3) and so on. In this way, the frontogenesis may become strong close to a region of highly negative EPV as observed in Figs. 5b and 5c, 10b, and 15b and 15c. CSI and, to a lesser extent, CI is continually generated and released over a smaller area. This likely led to the formation of heavy snowfall and large mesoscale snowbands, in each case, to the left of the region of midlevel drying and within the developing ''comma head'' with each storm.

Given the resolution, convective parameterization schemes, and 3- or 6-h periods between forecast times, it is difficult to ascertain the exact roles of CSI versus CI in producing mesoscale precipitation bands operationally. It has been postulated that CSI produces ascent that eventually triggers the release of CI (Xu 1986). This is often favored over warm frontal surfaces in a region of frontogenesis. Neiman et al. (1993) discussed a potential ''elevator'' and ''escalator'' ascent pattern for warm frontal zones associated with the release of both CI and CSI, respectively. The elevator portion of the ascent pattern in the warm frontal zone is associated with nearly vertical updrafts associated with the release of the CI. The escalator portion of the ascent pattern is associated with more slantwise updrafts associated with the release of CSI. It is possible that heavier precipitation may result when CI is present in addition to CSI as inferred from Seaman (1994). It is interesting to note that both the January and February cases showed regions of enhanced total snowfall in association with small layers of CI in the Meso Eta Model forecasts. Each case also exhibited a sharp cutoff to the heavy snowfall to the north and west. This might be attributable to the upper end of a CSI–CI updraft band (the top of the elevator or escaltor), which would place a region of heavy precipitation adjacent to a region of little or no precipitation.

c. Mesoscale snowband dissipation

When the midlevel low eventually forms a well-developed cyclonic circulation, the mesoscale snowband is postulated to get caught up in its circulation and fall to the west side of the midlevel low center, away from the source of dry advection aloft and reduction of EPV. Without the reduction of EPV, any CSI and CI present will be released and the atmosphere will return to a more stable state. This was most evident in the February and November cases in which the frontogenesis band at 700 hPa eventually migrated to the west side of the closed 700-hPa low circulation and weakened (Figs. 4d and 9c). The EPV also increased markedly with these two cases, at this time, indicating that the atmosphere became much more stable in conjunction with a weaker frontogenesis region. Unlike the January case, both the November and February cases attained a nearly vertical structure with the surface low and associated middle- to upper-level lows nearly collocated.

With a more vertical structure implied for the November and February cases, a more unidirectional northerly flow existed to the west of the cyclone center, which

was nearly parallel to the isotherms (equivalent barotropic). Since the flow was close to saturation through a deep layer, the reduction in EPV from (3) may have ceased near the frontogenetic region since the θ_e and θ surfaces became more coincident (not shown). This was becoming evident in the November case at the time period displayed in Fig. 16b. The November case was closer to a vertical structure at this time period than the other two cases in Fig. 16. Note that the frontogenesis was far removed from the region that favored a reduction in EPV, which was to the southeast near the dry tongue jet aloft (Fig. 16b). After the time period in Fig. 16b, the frontogenesis and associated mesoscale snowband diminished markedly in the November case. Without a mechanism to reduce EPV, it is also possible that the region of negative EPV was simply advected out of the region. This also may explain the marked increase in the EPV fields for two of the three cases that occurred to the west side of the upper-level lows.

d. Potential forecast applications

It is apparent from the cases in this study that the snowfall distribution from each cyclone did not decrease linearly away from the center of the surface low track. Instead, it was concentrated in a narrow region where the mesoscale snowband pivoted to the west of the midlevel low. The heaviest snowfall was not only concentrated into narrow mesoscale bands but also was displaced to the *northern and western edge of the precipitation shield* similar to the case presented in Sanders (1986). Thus, total snowfall dropped off dramatically to the north and west of the regions that received heavy snowfall. The mesoscale nature of the snowbands and the tendency for the bands of snow to be found near the northern and western edge of the precipitation shield presented major forecasting challenges.

The results of this study suggest that the potential for mesoscale snowbands with high snowfall accumulation rates, greater than 2.5 cm (1 in.) per hour, exist when a vertically deep layer of highly negative EPV forms in conjunction with a strong midlevel frontogenesis region. This frontogenesis and negative EPV region were found to the north of the developing midlevel (near 700 hPa) low during cyclogenesis. The deep layer of negative EPV (which was mainly CSI) was found above the isolated frontogenesis maximum in a cross section perpendicular to the isotherms, north of the surface low. The heaviest storm total snowfall was found to occur where the midlevel frontogenesis and negative EPV persisted on the west side of the midlevel low track. In addition, a very sharp cutoff to the storm total snowfall to the north and west of the heaviest storm total snowfall can be anticipated.

Snook (1992), Moore and Lambert (1993), and, more recently, Weismuller and Zubrick (1998) discuss ways to assess CSI operationally using EPV, θ_e, and M_g surfaces. The inspection of both EPV and θ_e–M_g cross sections is suggested in order to separate out CSI from CI assuming the atmosphere is near saturation. In the cases where CSI resides in conjunction with CI, gravitational accelerations dominate. In other words, the upright instability will dominate over the slantwise instability as discussed in the previous subsection.

The following is recommended to assess the potential for mesoscale snowband development and heavy snowfall associated with extratropical cyclones:

1) Use gridded model data from a mesoscale model, for example, Meso Eta, to diagnose the potential for mesoscale band formation.
2) Locate regions of frontogenesis between 850 and 500 mb in the baroclinic zone north of the developing low-level cyclone.
3) Examine a cross section of EPV and θ_{es} taken perpendicular to the isotherms and across the strongest region of frontogenesis.
4) A deep layer of highly negative EPV associated with a midlevel frontogenesis maximum signals the potential for mesoscale band formation and heavy snowfall in this region (assuming saturation is present).
5) If θ_{es} decreases with height in the negative EPV region, then CI is present, which may lead to extremely heavy snowfall rates. If θ_{es} increases with height in the negative EPV region, then CSI is present and mesoscale banding is likely with attendant enhanced snowfall rates.

Forecasters should anticipate a significant reduction in EPV near regions of drying aloft, especially when it occurs above a region of low-level moisture advection and warm advection. This is often the case during cyclogenesis when a midlevel dry tongue jet intersects the low-level easterly jet in the warm advection zone, north of a surface low, and forms the ''comma head'' signature of the cyclone. The generation of EPV can be easily assessed operationally by viewing the thermal wind vectors or thickness fields and relative humidity fields. Where the thermal wind vectors point in the same direction as the moisture gradient is where the reduction in EPV is found. In addition, software packages, like GEMPAK, have the capability to calculate the cross-product factor in (3) to determine the sign of the generation of EPV. Forecasters might be able to better locate regions susceptible to CSI by finding (in plane view) where EPV reduction is most persistent or strongest. Additionally, forecasters also can locate regions susceptible to CSI using EPV (calculated for a layer in the midtroposphere) viewed in plane view instead of in a cross section. Cross sections can then be taken across regions that display the most negative values of EPV in plane view.

A key finding in this study is *that finer-resolution, mesoscale models like the Meso Eta, can accurately simulate the meso-α environment conducive to intense mesoscale band formation without explicitly forecasting*

the band formation. Using frontogenesis and EPV from finer-resolution model data, forecasters can anticipate regions susceptible to intense mesoscale snow- or rainband formation, similar to how forecasters can anticipate regions conducive to (upright) convection. In a baroclinic environment (e.g., over a warm frontal surface), a layer of negative EPV signals that an instability is present (CSI and, at times, both CSI and CI). The presence of low-level or midlevel frontogenesis indicates that a lifting mechanism exists, which, by bringing the layer to saturation, can release the instability to form mesoscale precipitation bands. This is analogous to forecasters using convective available potential energy or the lifted index to determine how much upright instability is present for upright convection. A lifting mechanism is also essential to release the upright instability, which typically is a surface boundary or an upper-level short wave.

Forecasters should be aware that when the EPV is forecast to be low or negative by a numerical model, the frontal circulation that arises may be stronger and reduced to a smaller scale than the particular numerical model can resolve, especially the coarser-resolution, synoptic-scale models. Such models may have a difficult time handling symmetric instability and associated vertical motions. Thus, when deep layers of negative EPV are present in association with frontogenesis, forecasters should anticipate very heavy snowfall rates and watch for a distinct mesoscale snowband(s) to emerge in the northern portion of the precipitation shield on radar.

It has been a long-time practice of operational forecasters to diagnose the forcing of vertical motion from the omega equation through vorticity and temperature advections and, more recently, Q-vector divergence fields and frontogenesis. These fields all indicate where the atmosphere is being forced out of thermal wind (T–W) balance and where the ageostrophic flow and associated vertical motion is needed for restoration of T–W balance. The results of these cases suggest that examination of the forcing of vertical motion (frontogenesis) is only *a part of the problem* when assessing vertical motion from model output. *Inspection of how responsive the atmosphere is to any kind of forcing is just as important to the forecast process.*

The EPV fields govern how effective the vertical motion is at restoring T–W balance in the semigeostrophic form of the Sawyer–Elliassen equation (or the semigeostrophic form of the omega equation). EPV plays an analogous role to the static stability parameter in the quasigeostrophic (QG) omega equation, which governs the effectiveness of vertical motion at restoring T–W balance in a QG atmosphere. It is clear from these cases and from Weismuller and Zubrick (1998) that forecasters should assess *both* the forcing of vertical motion and how responsive the atmosphere is to forcing and if any instabilities (CSI or CI) are present. The models often capture the forcing of vertical motion well but can fall short in assessing vertical motion and precipitation from instabilities. This is an area where forecasters may be able to significantly improve upon model quantitative precipitation forecasts.

5. Conclusions

This study showed that frontogenetic forcing and negative EPV (which was primarily CSI) were important mechanisms for producing mesoscale bands of heavy snowfall in the three snowstorms. A narrow mesoscale band(s) of heavy snowfall formed in the north portion of each snowstorm, which was a major player in the distribution of heavy snowfall. The mesoscale snowbands produced high snowfall accumulation rates. The heaviest storm total snowfall was found close to where the mesoscale snowband persisted the longest (to the left of the 700-hPa low track).

A deep layer of negative EPV developed in conjunction with an intense midlevel frontogenesis maximum, north of each cyclone. The negative EPV was primarily associated with CSI as each case showed only limited regions of CI for short periods of time. As air ascended the isentropes north of each warm front, the CSI and, to a lesser extent, CI were released upon reaching saturation supporting the mesoscale snowbands and attendant heavy snowfall rates. Eventually, the frontogenesis band became associated with higher symmetric and upright stability (higher values of EPV), which is postulated to have diminished the frontal circulation and associated vertical motion.

EPV was found to be reduced in the zone where the dry tongue jet at midlevels overlaid the low-level easterly jet or CCB, north of the surface cyclone, and to the warm side of the frontogenesis maximum. This zone was characterized by strong differential moisture advection. Frontogenesis played an important role in reducing EPV by increasing the vertical wind shear, which, in turn, increased the differential moisture advection. With the continual reduction of EPV, a deep layer of negative EPV developed close to the intensifying region of frontogenesis. A synergy between frontogenesis and negative EPV was evident for each case from the Meso Eta Model forecasts. As the midlevel frontogenesis intensified, the EPV became highly negative and extended through a deep layer in the troposphere. This synergy between frontogenesis and negative EPV is postulated to be crucial for the development of the long-lived mesoscale snowbands with each case.

More research is needed to investigate the role of frontogenesis and EPV in forcing vertical motions and supporting banded precipitation in extratropical cyclones. Specifically, a more detailed understanding of the formation of highly negative regions of midlevel EPV and the associated intensification of the midlevel frontogenesis is needed. Does vertical advection of lower EPV from the low-levels play a role reducing the EPV at midlevels? The processes involved with the eventual increase in EPV and weakening of the front-

ogenesis region displayed in all three cases also needs to be further explored. More research is needed concerning the details and interactions between CSI and CI in mesoscale precipitation band formation. A better understanding of the roles of EPV and frontogenesis in mesoscale snowband formation will no doubt benefit forecasters, especially since mesoscale models are becoming more available to forecasters, which simulate these processes on a more realistic scale.

Acknowledgments. We would like to thank Kenneth Johnson, NWS Eastern Region, deputy chief, Scientific Services Division for his thorough initial review of this paper, which no doubt led to significant improvements. We are grateful to the anonymous reviewers and Dr. Steven E. Koch who played an important role in further clarifying and improving this paper. We are also grateful to Dr. John H. E. Clark and Dr. Gregory Forbes of The Pennsylvania State University; Jeff Waldstreicher, science and operations officer, NWS Binghamton, New York; and John LaCorte, forecaster, NWS State College, Pennsylvania; for their comments and initial review of this paper. We would also like to thank Ray Brady, senior forecaster NWS Binghamton, New York, for supplying some of the WSR-88D data for this study. This research was supported in part by UCAR Subaward S98-93857.

REFERENCES

Barnes, S. L., 1985: Omega diagnostics as a supplement to the LFM/MOS guidance in weakly forced convective situations. *Mon. Wea. Rev.,* **113,** 2122–2141.

Bennetts, D. A., and B. J. Hoskins, 1979: Conditional symmetric instability—A possible explanation of frontal rainbands. *Quart. J. Roy. Meteor. Soc.,* **105,** 945–962.

——, and J. C. Sharp, 1982: The relevance of conditional symmetric instability to the prediction of mesoscale rainbands. *Quart. J. Roy. Meteor. Soc.,* **108,** 595–602.

Black, T. L., 1994: The new NMC mesoscale eta model: Description and forecast examples. *Wea. Forecasting,* **9,** 265–278.

Bluestein, H. B., 1993: *Synoptic-Dynamic Meteorology in Midlatitudes.* Vol. II, *Observations and Theory of Weather Systems,* Oxford University Press, 594 pp.

Bosart, L. F., 1975: SUNYA experimental results in forecasting daily temperature and precipitation. *Mon. Wea. Rev.,* **103,** 1013–1020.

Browning, K. A., 1985: Conceptual models of precipitation systems. *Meteor. Mag.,* **114,** 293–319.

Cahir, J. J., J. M. Norman, and D. A. Lowry, 1981: Use of a real-time computer graphics system in analysis and forecasting. *Mon. Wea. Rev.,* **109,** 485–500.

Carlson, T. N., 1980: Airflow through midlatitude cyclones and the comma cloud pattern. *Mon. Wea. Rev.,* **108,** 1498–1509.

Dankers, T., 1994: Observing CSI bands using the WSR-88D. Postprints, *The First WSR-88D User's Conference,* Norman, OK, WSR-88D Operational Support Facility and NEXRAD Joint System Program Office, 159–168.

desJardines, M. L., K. F. Brill, and S. S. Schotz, 1991: GEMPAK user's guide. NASA Tech. Memo. 4260, National Aeronautics and Space Administration, 2021 pp. [Available from NASA Code NTT-4, Washington, DC 20546-0001.]

Dunn, L. B., 1991: Evaluation of vertical motion: Past, present, and future. *Wea. Forecasting,* **6,** 65–75.

Emanuel, K. A., 1979: Inertial instability and mesoscale convective systems. Part I: Linear theory of inertial instability in rotating viscous fields. *J. Atmos. Sci.,* **36,** 2425–2449.

——, 1983: The Lagrangian parcel dynamics of moist symmetric instability. *J. Atmos. Sci.,* **40,** 2368–2376.

——, 1985: Frontal circulations in the presence of small moist symmetric instability. *J. Atmos. Sci.,* **42,** 1062–1071.

Grumm, R. H., and D. J. Nicosia, 1997: WSR-88D observations of mesoscale precipitation bands over Pennsylvania. *Natl. Wea. Dig.,* **21,** 10–23.

Hoskins, B. J., and F. P. Bretherton, 1972: Atmospheric frontogenesis models: Mathematical formulation and solution. *J. Atmos. Sci.,* **29,** 11–37.

Jascourt, S. D., S. S. Lindstrom, C. J. Seaman, and D. D. Houghton, 1988: An observation of banded convective development in the presence of weak symmetric stability. *Mon. Wea. Rev.,* **116,** 175–191.

Klazura, G. E., and D. A. Imy, 1993: A description of the initial set of analysis products available from the NEXRAD WSR-88D system. *Bull. Amer. Meteor. Soc.,* **74,** 1293–1311.

Koch, S. E., 1984: The role of an apparent mesoscale frontogenetic circulation in squall line initiation. *Mon. Wea. Rev.,* **112,** 2090–2111.

Moore, J. T., and P. D. Blakeley, 1988: The role of frontogenetical forcing and conditional symmetric instability in the midwest snowstorm of 30–31 January 1982. *Mon. Wea. Rev.,* **116,** 2155–2171.

——, and T. E. Lambert, 1993: The use of equivalent potential vorticity to diagnose regions of conditional symmetric instability. *Wea. Forecasting,* **8,** 301–308.

Neiman, P. J., M. A. Shapiro, and L. S. Fedor, 1993: The life cycle of an extratropical marine cyclone. Part II: Mesoscale structure and diagnostics. *Mon. Wea. Rev.,* **121,** 2177–2199.

Nicosia, D. J., 1995: Diagnosing quasi-geostrophic forcing using PC-GRIDDS: A case study. National Weather Service, Eastern Region Tech. Attachment 95-2B, 18 pp. [Available from National Weather Service, Eastern Region Headquarters, Scientific Services Division, Airport Corporate Center, 630 Johnson Ave., Bohemia, NY 11716.]

O'Handley, C., and L. F. Bosart, 1989: Subsynoptic structure in a major synoptic-scale cyclone. *Mon. Wea. Rev.,* **117,** 607–630.

Petterssen, S., 1956: *Weather Analysis and Forecasting.* Vol. 1, McGraw-Hill, 428 pp.

Reuter, G. W., and M. K. Yau, 1990: Observations of slantwise convective instability in winter cyclones. *Mon. Wea. Rev.,* **118,** 447–458.

Ruscher, P. H., and T. P. Condo, 1996: Development of a rapidly deepening extratropical cyclone over land. Part II: thermodynamical aspects and the role of frontogenesis. *Mon. Wea. Rev.,* **124,** 1633–1647.

Sanders, F., 1973: Skill in forecasting daily temperature and precipitation: Some experimental results. *Bull. Amer. Meteor. Soc.,* **54,** 1171–1179.

——, 1986: Frontogenesis and symmetric instability in a major New England snowstorm. *Mon. Wea. Rev.,* **114,** 1847–1862.

——, and L. F. Bosart, 1985: Mesoscale structure in the Megalopolitan snowstorm of 11–12 February 1983. Part I: Frontogenetical forcing and symmetric instability. *J. Atmos. Sci.,* **42,** 1050–1061.

Seaman, C. J., 1994: A numerical study of nonlinear nonhydrostatic conditional symmetric instability in a convectively unstable atmosphere. *J. Atmos. Sci.,* **51,** 1352–1371.

Shields, M. T., R. M. Rauber, and M. K. Ramamurthy, 1991: Dynamical forcing and mesoscale organization of precipitation bands in a midwest winter cyclonic storm. *Mon. Wea. Rev.,* **119,** 936–964.

Snook, J. S., 1992: Current techniques for real-time evaluation of conditional symmetric instability. *Wea. Forecasting,* **7,** 430–439.

Wiesmueller, J. L., and R. H. Brady, 1993: A mid-Atlantic states rain

event: A review and comparison of techniques for assessing vertical motion fields. *Natl. Wea. Dig.*, **18,** 31–54.

——, and S. M Zubrick, 1998: Evaluation and application of conditional symmetric instability, equivalent potential vorticity, and frontogenetic forcing in an operational forecast environment. *Wea. Forecasting,* **13,** 84–101.

Wolfsberg, D. G., K. A. Emanuel, and R. E. Passarelli, 1986: Band formation in a New England snowstorm. *Mon. Wea. Rev.*, **114,** 1552–1569.

Xu, Q., 1986: Conditional symmetric instability and mesoscale rainbands. *Quart. J. Roy. Meteor. Soc.*, **112,** 315–334.

——, 1989: Extended Sawyer–Eliassen equation for frontal circulations in the presence of small viscous moist symmetric stability. *J. Atmos. Sci.*, **46,** 2671–2683.